JGR Earth Surface

RESEARCH ARTICLE
10.1029/2021JF006196

When and Where do Free Bars in Estuaries and Tidal Channels Form?

Niccolò Ragno[1], Nicoletta Tambroni[1], and Michele Bolla Pittaluga[1]

[1]Department of Civil, Chemical and Environmental Engineering, University of Genoa, Genoa, Italy

Key Points:

- A unified theoretical framework is proposed to study the incipient formation of bars in weakly converging tidal channels and estuaries
- In micro-tidal estuaries the width expansion toward the mouth promotes the formation of multiple bars
- Bars in tidal channels form far from the morphodynamic equilibrium state suggesting a dependency from the evolutionary history of the system

Correspondence to:
N. Ragno,
niccolo.ragno@edu.unige.it

Citation:
Ragno, N., Tambroni, N., & Bolla Pittaluga, M. (2021). When and where do free bars in estuaries and tidal channels form? *Journal of Geophysical Research: Earth Surface*, *126*, e2021JF006196. https://doi.org/10.1029/2021JF006196

Received 2 APR 2021
Accepted 20 SEP 2021

Abstract The incipient formation of free bars in weakly converging tidal channels and estuaries is mathematically framed within a unified two-dimensional shallow water and sediment mass balance model. The analysis is driven by the recognition that none of the theoretical models introduced so far account for the spatially varying character of the planform morphology, which characterizes estuaries and creeks forming networks in coastal wetlands and in the tide-dominated reaches of deltas. The problem is tackled by means of a linear stability analysis, by observing that width variations act on a spatial scale that is typically much longer than bars wavelength, allowing for an analytical treatment of the governing system of equations. We focus on two limit cases: first, the river transition into a micro-tidal sea (estuarine case); second, a tidal channel in the absence of a fluvial supply of freshwater and sediment (coastal case). In the estuarine case, bars arise as a result of an intrinsic instability of the equilibrium state. Width increases toward the mouth leading to channel shallowing, which in turn promotes the development of multiple bars. This effect is partially counteracted by the channel deepening produced by the tidal action, which tends to reduce bar growth and migration rate. In the coastal case, tidal bars form far from the equilibrium state of the system, adapting instantaneously to the evolving bed profile, which in turn affects channel flow conditions. Noteworthy, the model suggests that the spatial-temporal distribution of bars observed in nature reflects the evolutionary history of the system.

Plain Language Summary Tidal bars are large sediment waves characterized by a repetitive sequence of scour and deposition patches, which can spontaneously develop and migrate along estuaries and tidal channels. Studying their formation is important from a socio-economic perspective, as they affect navigation and the management of fluvial structures, and an ecosystem point of view, as they contribute to habitat diversity and richness. Here, we propose a theoretical model able to predict the conditions that favors the incipient formation of bars in two typical tidal environments: the transition of a river into the ocean ("estuarine case"), and a tidal channel in the absence of a landward river ("coastal case"). We show that these two cases can be framed within the same theoretical framework, retaining the complex interplay between the typically landward converging shape of channels and the influence of the tidal motion. The analysis of the model surprisingly reveals that tidal bars formation fundamentally depends from the history of the channel bed. This represents a key information to interpret field observations as well as to understand the response of bars due to natural and man-induced changes.

1. Introduction

Bars are mesoscale morphological patterns that arise from the interaction of sediment with fluid motion. They are sediment waves that typically form diagonal fronts, having wavelengths in the order of few channel widths and height of the order of the flow depth. A vast literature on river bars in fluvial systems has been growing in the last 50 years, involving theoretical studies (e.g., Bertagni & Camporeale, 2018; Callander, 1969; Colombini et al., 1987; Federici & Seminara, 2003; Fredsøe, 1978; Parker, 1976), experimental investigations (e.g., Fujita & Muramoto, 1985; Jaeggi, 1984; Lanzoni, 2000; Redolfi et al., 2020), field observations (e.g., Adami et al., 2016; Eekhout et al., 2013; Lewin, 1976; Rodrigues et al., 2015; Welford, 1994), and numerical modeling (e.g., Colombini & Tubino, 1991; Cordier et al., 2019; Defina, 2003; Siviglia et al., 2013). These studies show that bars arise spontaneously, in both gravel and sand bed rivers, as a result of an instability of the cohesionless bed, which tends to manifest when the width-to-depth ratio of the channel is larger than a critical value, which in turn depends on the river characteristics. They are downstream-migrating features, which are often organized in a single row (alternate bars) or, in the case of particularly wide and

shallow streams, in several rows (multiple row bars) (Seminara, 2010). Due to the autogenic character of their development, they are said to be "free," in opposition to the so-called "forced" bars, which are steady features that do not arise spontaneously but as a response to some physical constraint such as a geometrical variation (e.g., curvature, channel widening) or a local disturbance (e.g., the presence of an in-stream obstacle) (Bittner, 1995; Duró et al., 2016; Redolfi et al., 2016, 2021; Repetto et al., 2002; Seminara & Tubino, 1989; Struiksma & Crosato, 1989; Wu et al., 2011; Tambroni et al., 2019; Zolezzi et al., 2005).

The study of bars in tidal environments was initially restricted to a number of field observations (see the review of Dalrymple & Rhodes, 1995), receiving progressively increasing attention from the end of the last century. Linear stability theories (e.g., Blondeaux & Vittori, 2011; Garotta et al., 2006; Hepkema et al., 2019; Schramkowski et al., 2002; Schuttelaars & de Swart, 1999; Seminara & Tubino, 2001) show that bars forming in tidal channels characterized by the absence of a freshwater and sediment supply from an upstream river, arise due to an inherent instability process in a way similar to their fluvial counterpart, displaying however some peculiarities owing to the oscillatory character of the flow. In particular, in the absence of residual currents and/or an asymmetry of the tidal wave, tidal free bars do not exhibit any net migration, but oscillate back and forth during the tidal cycle. Numerical modeling has allowed further insights on the process of tidal bars formation, highlighting the development, over long timescales, of complex but stable riffle and pool patterns (Hibma et al., 2003, 2004; van de Lageweg & Feldman, 2018; van der Wegen & Roelvink, 2008; Yu et al., 2012). Nevertheless, these studies often consider tidal inlet systems and embayments characterized by values of the width-to-depth ratio in the order of 10^2. Consequently, they are not representative of a large class of tidal channels and creeks occurring in coastal wetlands networks and in the tide-dominated parts of deltas, where the width-to-depth ratio is typically one order of magnitude smaller (e.g., Marani et al., 2002).

In this work, we tackle the problem of analyzing the incipient formation of bars in landward converging micro-tidal streams (i.e., with tidal amplitude of one order of magnitude smaller than the average flow depth) by means of a two-dimensional mathematical model where relevant features of tidal environments, namely the common tide-induced seaward width expansion (e.g., Dalrymple & Choi, 2007; Nienhuis et al., 2018), and the unsteady character of the flow, are properly included. We identify two limit cases: first, the "estuarine case," concerning rivers debouching into an open sea (Figure 1a); second, the "coastal case," consisting of tidal channels distinguished by the total absence of a fluvial supply of freshwater and sediment (Figure 1b). Despite the scientific interest, this kind of problem bears a significant practical motivation. Indeed, the presence of migrating sequences of scour and deposit induces a preferential path for erosion on channel banks, affects channel navigation, the management of fluvial structures, and the feasibility of river regulation works.

The morphodynamics of estuaries, in which both the fluvial and tidal forcing concur to determine the flow field, has been poorly explored, being mainly limited to the investigation of the long-term equilibrium profile (e.g., Bolla Pittaluga et al., 2015; Guo et al., 2014; Seminara et al., 2012), along with some recent numerical simulations that have explored the morphodynamic evolution of large scale estuarine systems (Guo et al., 2015; van de Lageweg & Feldman, 2018). However, a theoretical study dealing with the formation of bars in these peculiar transitional systems is still absent. Comparatively, tidal bars in the coastal case received a considerable amount of attention (see the references mentioned hereinabove). Nevertheless, a set of various fundamental issues are still unsettled, closely tied with field and empirical evidences showing how sediment transport in tide-dominated channels tends to vanish as the bed profile approaches its equilibrium state, in turn preventing bars formation in such conditions (e.g., Friedrichs, 1995; Lanzoni & Seminara, 2002; Tambroni et al., 2005). One is then readily faced with a natural series of questions: what are the main differences between bars formed in the coastal case with respect to the estuarine case? If tidal bars do not form at equilibrium, when do they arise? Is their spatial and temporal development affected by the evolutionary process of the system?

In chapter 2, we show that the study of tidal bars in estuaries and tidal channels can be framed within the same theoretical framework. The problem can be tackled mostly analytically by means of a perturbation approach recognizing that typically, variations of the channel geometry affect flow and bed topography on a spatial scale that is much longer than bars wavelength. The main novelty of the work consists in the model proposed: a semianalytical approach allows to detect and isolate the main physical mechanisms and factors controlling the process of incipient bars formation, which we handled by means of a linear stability analysis

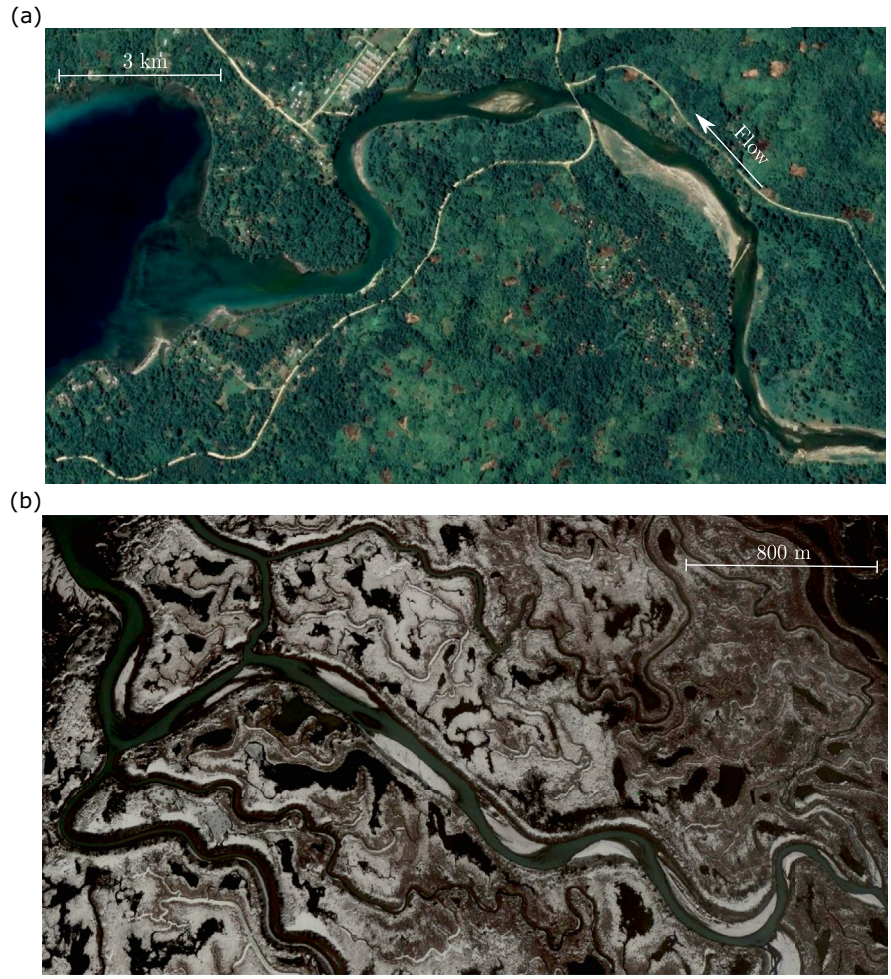

Figure 1. (a) Satellite image of a micro-tidal estuary along the coast of Papua Nuova Guinea (6°35′S, 147°49′E), with the peculiar funnel-shape planimetric morphology. (b) Alternate bars in a tidal channel bounded by tidal flats in the Alaska region (USA, 60°26′N, 145°30′W). From Google Earth, Digital Globe (2021).

in chapter 3. Subsequently, the model is applied to give an answer to the above-raised questions (chapter 4). We observe that, whereas bars in micro-tidal estuaries arise due to an intrinsic instability of an equilibrium state of the system similarly to their fluvial counterpart, bars in tidal channels crucially depend on the past and actual temporal stage of the bed profile in its evolution toward equilibrium. We discuss the implications of our findings along with the main limitations of the model in chapter 5. Finally, chapter 6 is devoted to some concluding remarks.

2. Formulation of the Problem

The aim of this chapter is to build a unified physically based model to study bars formation in micro-tidal estuaries and tidal channels. To achieve this goal, we place in a two-dimensional framework relying on a depth-averaged shallow water formulation in accordance with many previously developed bars models (e.g., Callander, 1969; Colombini et al., 1987; Parker, 1976). We consider the flow in a well-mixed tidal stream with a cohesionless bed consisting of homogeneous sediment with median grain size d^* (from hereinafter the superscript * denotes dimensional quantities), bounded seaward by a tidal sea. The possible effect of wind waves is herein neglected, with the banks assumed to be nonerodible. A Cartesian reference frame is adopted, with x^* and y^* indicating the longitudinal and transversal coordinate, respectively, with $x^* = 0$ at the tidal sea and increasing upstream.

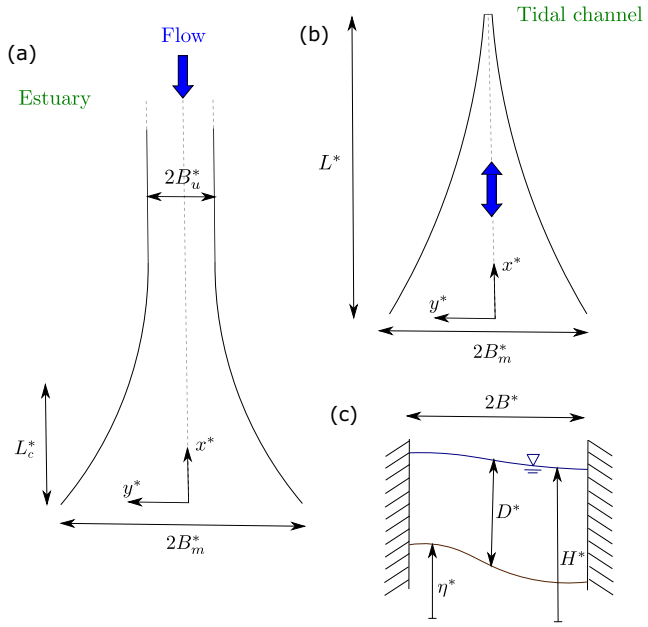

Figure 2. Geometrical scheme of the micro-tidal estuary adopted in the present formulation. The planimetric view describes both the (a) estuarine case, and (b) the coastal case, in which the bidirectional flow is highlighted by the blue arrow. The latter case is characterized by a finite length L^*. The convergence length L_c^* is the distance over which the width at the mouth reduces by a factor e (i.e., $e \simeq 2.72$) (e.g., Davies & Woodroffe, 2010). Panel (c) presents a detail of a reference cross-section, where η^* denotes the bed elevation, given by the difference between the water surface elevation H^* and the flow depth D^*.

Spatial variations of the channel geometry are taken into account, as sketched in Figure 2. In natural tidal environments, it is commonly observed a gradual width increase toward the mouth, which can be adequately approximated by an exponential law (e.g., Davies & Woodroffe, 2010; Langbein, 1963; Lanzoni & D'Alpaos, 2015; Lanzoni & Seminara, 1998; Pillsbury, 1940):

$$B^* = B_u^* + (B_m^* - B_u^*)\exp\left(-\frac{x^*}{L_c^*}\right), \tag{1}$$

where L_c^* is the so-called convergence length, B_m^* the halfwidth at the mouth, and B_u^* the halfwidth asymptotically reached upstream that is not affected by tidal processes (from hereinafter we indicate with the suffixes $_u$ and $_m$, the values of a variable in the upstream river and at the mouth, respectively). Equation 1 holds for both the coastal and estuarine case; however, the former is characterized by a vanishing value of the quantity B_u^* and by a finite length L^*, while the latter is assumed to be infinitely long landward.

It is worth to observe that in the present problem different spatial scales come into play: first, the planimetric dimension of bars is related to the channel width; accordingly we can consider a characteristic width B_r^*, coinciding with B_u^* and B_m^* in the estuarine and coastal case, respectively (from hereinafter the subscript $_r$ denotes a reference scaling quantity). Second, the convergence length L_c^* governs the rate of variation of the smooth finite widening toward the mouth (see Equation 1). Third, in riverine estuaries hydrodynamic processes are affected by the sea level variations over a distance, the so-called backwater length L_b^*, defined as the ratio between the uniform flow depth D_u^* and the bed slope S (e.g., Paola & Mohrig, 1996). The backwater length is a key quantity for the investigation of various processes in coastal systems, such as the formation of stratigraphic patterns or avulsion phenomena (i.e., a sudden event where flow diverts out of an established river channel into a new path) (e.g., Chatanantavet et al., 2012; Fernandes et al., 2016; Jerolmack, 2009; Slingerland & Smith, 2004). By performing an analysis of several natural tidal streams (see Table 1), we note that in estuaries B_r^* is typically much smaller than both L_c^* and L_b^*, which in turn have values of the same magnitude. Differently, in tidal channels the convergence length has usually the same order of the finite length of the channel L^*. Consequently, assuming L_b^*, L^* and L_c^* in the order of 10^3 m–10^6 m and B_r^* in the order of 10^2 m–10^3 m, means that the ratio of these different spatial quantities is typically well below unity. This observation suggests to introduce a parameter γ:

$$\gamma = \frac{B_r^*}{L_r^*} \ll 1, \tag{2}$$

which expresses the ratio between B_r^* and a characteristic length scale of spatial variations L_r^*.

Summarizing, in tidal streams two spatial scales are found to play a crucial role to study bedforms formation:

$$\underbrace{x = \frac{x^*}{B_r^*}}_{\text{Short bar scale}}, \qquad \underbrace{\xi = \frac{x^*}{L_r^*} = \gamma x}_{\text{Long channel scale}}, \tag{3}$$

with γ that governs how flow and bed topography are affected by width variations. We highlight that channel widening is smooth in the sense of Equation 2, which sets the upper bound of validity of the present formulation (i.e., $\gamma \simeq \mathcal{O}(1)$). Thus, the model is expected to not be valid in the case of strongly convergent tidal channels (see e.g., Friedrichs & Aubrey, 1994; Lanzoni & Seminara, 1998) or topographic expansions (e.g., Shaw et al., 2018; Sittoni et al., 2014; Tambroni et al., 2019). In order to simplify the formulation, it is useful to represent the physical domain into an equivalent rectangular one by introducing the following transversal coordinate $\hat{y}$ (e.g., Hall, 2005; Repetto et al., 2002):

Table 1
Relevant Parameters for Different Tidal Channels in Natural and Laboratory Settings

Case	Type	a^* (m)	D_r^* (m)	L_r^* (km)	L_c^* (km)	B_r^* (m)	a (−)	γ (−)
Venice#1[a]	Coastal	0.4	4	4.3	3.9	121	0.1	0.028
Venice#2[a]	Coastal	0.4	2.8	2.1	1.3	109	0.14	0.053
Venice#3[a]	Coastal	0.4	2.6	1.6	1.3	45	0.15	0.028
Venice#4[a]	Coastal	0.4	3.8	1.9	1.8	63	0.11	0.032
Exp#2[b]	Coastal	0.026	0.09	0.022	0.031	0.4	0.29	0.018
Rotterdam[c]	Coastal	1	11.5	37	56	1400	0.09	0.038
Tees[c]	Coastal	1.5	7.5	14	5.5	600	0.2	0.043
Magra[d]	Estuarine	0.15	3.9	39	1.5	60	0.04	0.003
Columbia[e]	Estuarine	1	10	240	25	1500	0.1	0.006
Elbe[e]	Estuarine	2	10	77	42.0	250	0.2	0.003
Fraser[e]	Estuarine	1.5	9	108	215	750	0.17	0.007
St. Lawrence[e]	Estuarine	2.5	7	330	183	19,000	0.36	0.057

[a]Sources: Toffolon and Lanzoni (2010). [b]Tambroni et al. (2005). [c]Todeschini et al. (2008). [d]Bolla Pittaluga et al. (2014). [e]Lanzoni and Seminara (1998).

$$\hat{y} = \frac{y}{B}, \qquad -B \le y \le B, \tag{4}$$

so that $\hat{y}$ runs between (− 1,1).

We now introduce the St. Venant equations of shallow water flow, coupled with the Exner equation stating the sediment mass conservation. In the formulation of the momentum balance, Coriolis forces and possible effects due to density currents are neglected, as usually appropriately done in the present kind of problems (see e.g., de Swart & Zimmerman, 2009; Seminara & Tubino, 2001; Ter Brake & Schuttelaars, 2011). The recognition of the two spatial scales (Equation 3), along with the coordinate transformation (Equation 4), lead to the following system of partial differential equations:

$$\varpi\frac{\partial U}{\partial t} + U\frac{\partial U}{\partial x} + \gamma U\frac{\partial U}{\partial \xi} - \gamma U\frac{\hat{y}}{B}\frac{dB}{d\xi}\frac{\partial U}{\partial \hat{y}} + \frac{V}{B}\frac{\partial U}{\partial \hat{y}} + \Psi\frac{\partial H}{\partial x} + \gamma\Psi\frac{\partial H}{\partial \xi} - \gamma\Psi\frac{\hat{y}}{B}\frac{dB}{d\xi}\frac{\partial H}{\partial \hat{y}} + \beta_r\frac{\tau_x}{D} = 0, \tag{5a}$$

$$\varpi\frac{\partial V}{\partial t} + U\frac{\partial V}{\partial x} + \gamma U\frac{\partial V}{\partial \xi} - \gamma U\frac{\hat{y}}{B}\frac{dB}{d\xi}\frac{\partial V}{\partial \hat{y}} + \frac{V}{B}\frac{\partial V}{\partial \hat{y}} + \frac{\Psi}{B}\frac{\partial H}{\partial \hat{y}} + \beta_r\frac{\tau_y}{D} = 0, \tag{5b}$$

$$\varpi\frac{\partial D}{\partial t} + \frac{\partial}{\partial x}(UD) + \gamma\frac{\partial}{\partial \xi}(UD) - \gamma\frac{\hat{y}}{B}\frac{dB}{d\xi}\frac{\partial}{\partial \hat{y}}(UD) + \frac{1}{B}\frac{\partial}{\partial \hat{y}}(VD) = 0, \tag{5c}$$

$$\frac{\partial}{\partial t}(\Psi F_r^2 H - D) + \frac{\Upsilon}{\varpi}\left(\frac{\partial q_{sx}}{\partial x} + \gamma\frac{\partial q_{sx}}{\partial \xi} - \gamma\frac{\hat{y}}{B}\frac{dB}{d\xi}\frac{\partial q_{sx}}{\partial \hat{y}} + \frac{1}{B}\frac{\partial q_{sy}}{\partial \hat{y}}\right) = 0, \tag{5d}$$

where the variables of the problem are expressed in a dimensionless form to remove scaling effects. We have conveniently defined:

$$(U^*, V^*) = U_r^*(U, V), \qquad D^* = D_r^* D, \qquad H^* = H_r^* H, \tag{6a}$$

$$(\tau_x^*, \tau_y^*) = \rho^* U_r^{*2}(\tau_x, \tau_y), \qquad (q_{sx}^*, q_{sy}^*) = \sqrt{\Delta g^* d^{*3}}(q_{sx}, q_{sy}), \qquad t^* = t\sigma^{*-1}, \tag{6b}$$

where (U^*, V^*) are the longitudinal and transversal components of the depth-averaged velocity vector, (τ_x^*, τ_y^*) the bed shear stresses, (q_{sx}^*, q_{sy}^*) the sediment flux components per unit width, H^* is the water surface elevation above some reference level, D^* is the flow depth, t^* is time, ρ^* is the water density, $\sigma^* = 2\pi/T^*$ is the angular frequency of the tidal wave with period T^*, g^* is the gravity acceleration, and Δ is the relative

submerged sediment density (herein set equal to 1.65). Furthermore, a number of dimensionless parameters arise:

$$\varpi = \frac{\sigma^* B_r^*}{U_r^*}, \qquad \Upsilon = \frac{\sqrt{\Delta g^* d^{*3}}}{(1-p) D_r^* U_r^*}, \qquad \beta_r = \frac{B_r^*}{D_r^*}, \qquad \Psi = \frac{g^* H_r^*}{U_r^{*2}}, \tag{7}$$

where ϖ is the ratio between the time required for a tidal wave to run along a reach of length B_r^* and the tidal period, β_r is the channel aspect ratio (i.e., half width-to-depth ratio), Υ is the ratio between the typical hydrodynamic and morphological timescale, and p is the sediment porosity.

Different scaling quantities distinguish estuaries and tidal channels. In the estuarine case, H_r^*, which measures the scale of variations of the free surface, is assumed to coincide with D_u^* that, along with U_u^*, represent the values that would occur in uniform flow conditions for a straight channel with width $2B_u^*$. As a consequence, the parameter Ψ is equal to $1/F_u^2$, with $F_u = U_u^*/\sqrt{g^* D_u^*}$ the Froude number. Essentially, the latter scaling states that the estuary is dominated by riverine processes, with variations of the water surface elevation that are proportional to the kinetic energy of the current in the momentum balance (i.e., $\propto U_u^{*2}/g^*$). Differently, in tidal channels normal flow conditions become meaningless due to the absence of an upstream riverine reach, and an appropriate re-scaling is needed; an arguable choice, is to scale the flow depth with the depth at the mouth D_m^*, employing the tidal amplitude a_* to scale the variations of the free surface, and considering U_r^* as the speed of a small amplitude inviscid tidal wave (i.e., $U_r^* \propto \sqrt{g^* D_m^*}$) (Seminara et al., 2010). The parameter Ψ is found to coincide with the ratio between the scaled tidal amplitude $a = a^*/D_r^*$ and the square of the Froude number F_r^2, noting that for values typical of micro-tidal channels this ratio is of order one. In overall, this scaling physically translates in values of D_r^* ranging in the order of 1 m–10 m, $U_r^* \simeq 1$ m/s (i.e., $F_u^2 \simeq 10^{-2}$), and $a^*/D_r^* \simeq 10^{-1}$, which are common in typical micro-tidal estuaries and tidal channels found in nature (Friedrichs & Aubrey, 1994; Lanzoni & Seminara, 1998; Seminara et al., 2001). In addition, we note that ϖ and Υ are typically small parameters since ϖ is found to fall in the range 10^{-3}–10^{-1} for a semidiurnal tide (i.e., $\sigma^* \simeq 10^{-4}$ s^{-1}), whereas Υ is about 10^{-5} to 10^{-6} as the grain size in tidal environments typically falls in the range of medium-fine sand (i.e., $d^* \simeq 10^{-4}$ m).

Closure relationships are required to express the shear stress and sediment transport rate in terms of the governing variables of the problem (i.e., U, V, D, H). This is achieved through a "local equilibrium" approximation, which is justified by the slowly varying character of the flow field either in space and time (e.g., Redolfi et al., 2021; Tubino, 1991). In other words, (τ_x, τ_y) and (q_{sx}, q_{sy}) are computed in terms of the local value of the flow variables. Thus, following a widely adopted procedure the bottom stress vector is defined as:

$$\boldsymbol{\tau} = (\tau_x, \tau_y) = C_f (U, V)(U^2 + V^2)^{\frac{1}{2}}, \tag{8}$$

where C_f is a friction coefficient, estimated through the Manning-Strickler formula:

$$C_f^{-1/2} = C_{fr}^{-1/2} D^{1/6}, \quad C_{fr}^{-1/2} = \frac{k_s^* D_r^{*1/6}}{\sqrt{g^*}}, \tag{9}$$

with k_s^* the Gauckler-Strickler coefficient.

The Einstein scaling (Einstein, 1950) is used to express the sediment transport rate in terms of a sediment load function Φ, computed through the formula proposed by Engelund and Hansen (1967), which includes the contribution of both the bedload and suspended load fraction:

$$\Phi = 0.05 C_f^{-1} \theta^{5/2}, \qquad \theta = \frac{|\boldsymbol{\tau}^*|}{\rho^* \Delta g^* d^*}, \tag{10}$$

with θ the Shields parameter. Following a classic argument, the direction of the local sediment transport vector, given by the angle χ, accounts for two contributions (see e.g., Blondeaux & Seminara, 1985; Engelund, 1981; Parker, 1984): first, the direction of the flow velocity vector; second, the correction due to the downslope pull of gravity in the transverse direction, whose magnitude is quantified by the empirical parameter r. Thus, we define:

$$\boldsymbol{q_s} = (q_{sx}, q_{sy}) = (\cos\chi, \sin\chi)\Phi, \tag{11a}$$

$$\sin\chi = V(U^2 + V^2)^{-1/2} - \frac{r}{\beta_r\sqrt{\theta}}\frac{\partial}{\partial y}(\Psi F_r^2 H - D), \tag{11b}$$

with r assuming values between 0.3 and 0.6 (e.g., Olesen, 1983; Talmon et al., 1995).

Finally, to solve system (Equations 5a–5d) proper boundary conditions have to be imposed. First of all, we express the physical requirement the channel walls to be impermeable both to flow and sediment fluxes:

$$-\gamma U\frac{dB}{d\xi} \pm V = 0, \qquad \hat{y} = \pm 1, \tag{12a}$$

$$-\gamma q_{sx}\frac{dB}{d\xi} \pm q_{sy} = 0, \qquad \hat{y} = \pm 1, \tag{12b}$$

where we note that the quantity $-\gamma(U, q_{sx})dB/d\xi$ derives from the expression of the unit vector locally normal to the banklines. At the channel mouth, the presence of a tidal sea induces an oscillation of the free surface (a^*), which as anticipated, is assumed to be small with respect of D_r^* in both the estuarine and coastal case. On the contrary, the definition of the landward boundary condition is case specific and deserves a more thorough discussion that we postpone to the next chapter.

3. Linear Stability Analysis

The theoretical model developed in the previous chapter is general and, with the definition of proper boundary conditions, can be easily employed to study the flow and bed topography evolution in a wide range of environmental settings. In the following, we draw the attention to the main purpose of the present work: investigating bars formation in tidal streams by means of a linear stability analysis.

In general, a linear stability analysis is a mathematical tool that allows to investigate the conditions whereby some (undisturbed) reference state of the system loses stability to perturbations small enough for linearization to be a valid approximation (e.g., Seminara, 1998). Typically, for an infinitely long straight channel fed upstream by a constant water discharge, the plane uniform turbulent flow over a sloping bed, which corresponds to equilibrium conditions, can be appropriately chosen as a basic state (e.g., Colombini et al., 1987; Parker, 1976; Seminara, 1998). This means that if we imagine the basic uniform flow to be perturbed by some (strictly infinitesimal) disturbances, under suitable circumstances we will observe the formation of sequences of bars in a periodic fashion, which are unaffected by the conditions at the inlet and outlet boundary of the domain.

The picture is made more complex in the case of tidal streams due to the combined effects of both channel widening and tidal motion. As a consequence, in the present problem the basic flow is no longer uniform, being in general a function of time and space. For example, this concept can be easily understood by considering a river approaching a standing body of water (e.g., a lake or a sea). Depending on the flow conditions, a spatial acceleration/deceleration follows a decrease/increase of the water surface elevation, which is ultimately fixed by the level of the receiving basin. The length over which the flow is no longer uniform, is the previously defined backwater length L_b^*.

Let us consider a perturbed flow and bed topography of the form:

$$U = U_0(\xi, t) + \epsilon U_1(x, \xi, \hat{y}, t) + \mathcal{O}(\epsilon\gamma, \epsilon^2), \tag{13a}$$

$$V = \gamma V_0(\xi, \hat{y}, t) + \epsilon V_1(x, \xi, \hat{y}, t) + \mathcal{O}(\epsilon\gamma, \epsilon^2), \tag{13b}$$

$$D = D_0(\xi, t) + \epsilon D_1(x, \xi, \hat{y}, t) + \mathcal{O}(\epsilon\gamma, \epsilon^2), \tag{13c}$$

$$H = H_0(\xi, t) + \epsilon H_1(x, \xi, \hat{y}, t) + \mathcal{O}(\epsilon\gamma, \epsilon^2), \tag{13d}$$

where ϵ is the small (strictly infinitesimal) amplitude of the disturbance, and the subscripts $_0$ and $_1$ indicate the basic state and the first order perturbation, respectively.

A few words are required to explain the structure of the expansion (Equations 13a–13d). Tidal sea oscillations and spatial variations of the banklines deviate the response of the channel from the uniform flow conditions. In turn, those variations are assumed to be gradual along the spatial coordinate ξ, as indicated by the magnitude of the parameter γ. Typical values of γ, as reported in Table 1, suggest that the latter parameter is of the order 10^{-2}. Physically, this means that at the spatial scale of bars the flow is analogous to the one that occurs in an infinitely long channel of the same (local) width ($2B^*$) (Hall, 2005). Hence, as suggested by several authors (e.g., Tambroni et al., 2017; van der Wegen & Roelvink, 2008), as a first approximation the morphodynamic response adjusts to the local channel characteristics, which globally, are slowly varying functions of time and space. It is worth noticing that in Equation 13b, the principal component of the cross-velocity V_0 is multiplied by γ; physically, we are assuming the basic flow to be one-dimensional, though allowing a possible (small) correction induced by channel widening, as suggested by the boundary conditions (Equations 12a and 12b). Furthermore, the nonlinear interaction between the "free" (ϵ) and the "forced" perturbations due to spatial width variations (γ) is herein neglected (see the detailed works by Luchi et al., 2011; Monegaglia et al., 2019; Seminara & Tubino, 1989; Tubino & Seminara, 1990). Ultimately, we observe that the definition of the basic state as a general function of both the spatial and temporal coordinate represents a main novelty in the context of previously developed linear stability analysis for bars formation. Its structure, which enables to unify the two extreme cases of tidal channels and estuaries in the same theoretical framework, will be discussed in the next section.

3.1. The Basic State

Let us substitute the expansion (Equations 13a–13d) into system (Equations 5a–5d) and retain just the leading order terms. By performing a transversal integration of the flow and sediment mass conservation equations between -1 and 1, using the boundary conditions (Equations 12a and 12b), and ensuring the coupling with the momentum equation along ξ, we find:

$$\varpi \frac{\partial U_0}{\partial t} + \gamma U_0 \frac{\partial U_0}{\partial \xi} + \gamma \Psi \frac{\partial H_0}{\partial \xi} + \beta_r C_{fr} \frac{U_0 |U_0|}{D_0^{4/3}} = 0, \tag{14a}$$

$$\frac{\varpi}{\gamma} \frac{\partial D_0}{\partial t} + \frac{\partial}{\partial \xi}(U_0 D_0) + \frac{1}{B} \frac{dB}{d\xi}(U_0 D_0) = 0, \tag{14b}$$

$$\frac{\partial}{\partial t}(\Psi F_r^2 H_0 - D_0) + \gamma \frac{\Upsilon}{\varpi} \frac{\partial}{\partial \xi}(B q_{sx0}) = 0, \tag{14c}$$

which represents a set of partial differential equations in the unknowns (U_0, D_0, H_0). It is worth noticing that: first, the system (Equations 14a–14c) is nonlinear; second, by applying appropriated boundary conditions it can be solved analytically, taking advantage that there is a third small parameter in the formulation, the scaled tidal amplitude. In order to better investigate the nature of the basic state, we analyzed separately the estuarine and coastal case.

3.1.1. Estuarine Case

The formation of a backwater profile as the river approaches the tidal sea, constrains us to seek for a suitable definition of the equilibrium conditions, whose solution represents the basic state to be perturbed. Specifically, the Exner Equation 14c provides the basis to determine a tidally averaged equilibrium, achieved when the bed elevation does not experience any net aggradation/degradation in a tidal cycle (Bolla Pittaluga et al., 2015). At the upstream end, normal flow conditions are assumed to take place, and a steady freshwater discharge per unit width q_u^* along with a bed slope S are given as external inputs. System (Equations 14a–14c) can then be solved analytically by means of a perturbation approach, as first derived by Seminara et al. (2012). They recognize that an asymptotic solution can be found by expanding each unknown physical variable of the problem in terms of the small parameter a, the scaled tidal amplitude (for the complete solution, see Appendix A). A comparison with numerical simulations shows that the analytical solution provides satisfactorily results up to $a \simeq 0.3$ (Bolla Pittaluga et al., 2015; Seminara et al., 2012).

3.1.2. Coastal Case

We now proceed to investigate the basic state of a tidal channel in which no freshwater and sediment discharges are supplied from the landward end of the channel ($\xi = 1$). A number of field observations and numerical studies have highlighted that tidal channels tend asymptotically to an equilibrium condition characterized by a shoaling bed profile, shallowing landward, with a nearly vanishing net sediment flux in a tidal cycle (e.g., Friedrichs, 1995; Lanzoni & Seminara, 2002; Todeschini et al., 2008), a behavior further supported by the laboratory experiments of Tambroni et al. (2005). This means that at equilibrium, the maximum velocity attained throughout the channel tends to coincide with the critical velocity for sediment motion. Such a state is called by Seminara et al. (2010) a "static" equilibrium. In real world a static equilibrium is hardly reached due to various mechanisms that cause departure from this ideal condition, and a "dynamic" equilibrium criterion was suggested by several authors (e.g., Friedrichs & Aubrey, 1996; Pritchard & Hogg, 2003), meaning that at equilibrium, the flow velocity must be spatially constant but may have a value slightly greater than that required for incipient sediment motion.

Regardless the equilibrium criterion that we may pursue, a fundamental conceptual problem arises: do tidal bars form at equilibrium? Or in other words, is the equilibrium condition, either static or dynamic, the proper basic state to study bar formation in tide-dominated channels? From what it has been introduced so far, it seems quite evident that even if the dynamic equilibrium criterion is accepted, bars hardly form due to the very weak currents (i.e., low values of the sediment flux as the Shields number tends to vanish), with the timescale of the transient growing process being extremely large. This subtle problem was recognized implicitly in the numerical tests carried out by van der Wegen and Roelvink (2008), who were constrained to arbitrarily linearize the starting initial bed profile for their simulations. Furthermore, a linear bed profile is a commonly employed initial condition for numerical performances, and represents the basic state in several previously developed linear stability analysis focusing on short tidal embayments (e.g., Schuttelaars & de Swart, 1999; Ter Brake & Schuttelaars, 2011; van Leeuwen & de Swart, 2001).

In order to build a proper theoretical framework, we rely on the asymptotic approach proposed by Seminara et al. (2010), which is appropriated for the short tidal channels (i.e., the channel length is much shorter than the tidal wavelength) typically observed in coastal wetlands and lagoons at equilibrium. The bulk of the analytical technique employed by the latter authors, consists in dividing the channel into two regions: an outer region, where the flow depth (D^*) scales with the inlet depth (D_m^*), and a smaller inner region adjacent to the moving shoreline, which behaves as a boundary layer, where a proper re-scaling is needed. As in the present problem we are not in equilibrium conditions, D^* scales in every part part of the domain with D_m^*. Consequently, the upstream boundary condition is assumed to behave as an impermeable barrier (i.e., $U\,|_{\xi=1} = 0$). At the leading order, Seminara et al. (2010) found the following expression for the velocity field:

$$U_0 = \frac{\Lambda L_c}{D_0}\left[1 - \exp\left(\frac{\xi - 1}{L_c}\right)\right]\frac{df}{dt}, \quad L_c = \frac{L_c^*}{L^*}, \quad \Lambda = \frac{L^*\sigma^*}{a\sqrt{g^* D_m^*}}. \tag{15}$$

We note that differently from the estuarine case, the basic flow is a function of both space and time. Velocity attains its maximum at the channel mouth, until reaching the zero value at the channel end. Furthermore, we highlight that despite Equation 15 has been formally derived in the outer region of a tidal channel at equilibrium, its validity may be in principle extended to any tidal channel configuration even far from equilibrium provided the flow depth scales with the inlet depth.

3.2. Linear Order

We then move to the order ϵ, namely the linear perturbation state. The stability analysis employed follows a classical argument, and it is identical for both the estuarine and coastal case. We just observe that due to the linear nature of the analysis, as stated by the expansion (Equations 13a–13d), terms of order $\mathcal{O}(\epsilon\gamma)$ that account for nonlinear effects on (free) bars formation, are neglected. Thus, the boundary conditions are defined as:

$$V_1 = q_{sy1} = 0, \qquad \hat{y} = \pm 1, \tag{16a}$$

$$H_1|_{\xi=0} = 0, \quad (U_0 D_1 + D_0 U_1)|_{\xi\to\infty} = 0, \qquad \text{Estuarine case} \tag{16b}$$

$$H_1\,|_{\xi=0}=0,\quad U_1|_{\xi=1}=0. \qquad \text{Coastal case} \tag{16c}$$

The above conditions allow for the expansion of the perturbations in Fourier series along the transverse-direction ($\hat{y}$) as follows:

$$\{U_1,D_1,H_1\}=\{\mathcal{U}_1(x,\xi,t),\mathcal{D}_1(x,\xi,t),\mathcal{H}_1(x,\xi,t)\}G_m(\hat{y}), \tag{17a}$$

$$V_1=\mathcal{V}_1(x,\xi,t)P_m(\hat{y}), \tag{17b}$$

where the transverse structure of the different modes (m) reads:

$$G_m(\hat{y})=\sin\left(\frac{m\pi\hat{y}}{2}\right),\quad P_m(\hat{y})=\cos\left(\frac{m\pi\hat{y}}{2}\right),\quad (m\in\text{odd}), \tag{18a}$$

$$G_m(\hat{y})=\cos\left(\frac{m\pi\hat{y}}{2}\right),\quad P_m(\hat{y})=\sin\left(\frac{m\pi\hat{y}}{2}\right),\quad (m\in\text{even}). \tag{18b}$$

By substituting from (Equations 13a–13d) and (Equations 17a and 17b) into the governing differential system (Equations 5a–5d), and performing the linearization procedure, we obtain:

$$\varpi\frac{\partial\mathcal{U}_1}{\partial t}+U_0\frac{\partial\mathcal{U}_1}{\partial x}+\Psi\frac{\partial\mathcal{H}_1}{\partial x}+\frac{\beta_r C_{fr}U_0|U_0|}{D_0^{4/3}}\left[2\frac{\mathcal{U}_1}{U_0}-\frac{4}{3}\frac{\mathcal{D}_1}{D_0}\right]=0, \tag{19a}$$

$$\varpi\frac{\partial\mathcal{V}_1}{\partial t}+U_0\frac{\partial\mathcal{V}_1}{\partial x}+M\Psi\mathcal{H}_1+\frac{\beta_r C_{fr}|U_0|}{D_0^{4/3}}\mathcal{V}_1=0, \tag{19b}$$

$$\varpi\frac{\partial\mathcal{D}_1}{\partial t}+D_0\frac{\partial\mathcal{U}_1}{\partial x}+U_0\frac{\partial\mathcal{D}_1}{\partial x}-MD_0\mathcal{V}_1=0, \tag{19c}$$

$$\frac{\partial}{\partial t}(\Psi F_r^2\mathcal{H}_1-\mathcal{D}_1)+\Phi_r\frac{\Upsilon}{\varpi}\frac{U_0^5}{\sqrt{D_0}}\left[\frac{5}{|U_0|}\frac{\partial\mathcal{U}_1}{\partial x}-\frac{1}{2D_0}\frac{\partial\mathcal{D}_1}{\partial x}-M\frac{\mathcal{V}_1}{|U_0|}+\frac{D_0^{1/6}}{|U_0|}M^2R(\Psi F_r^2\mathcal{H}_1-\mathcal{D}_1)\right]=0, \tag{19d}$$

where $M=(-1)^{m-1}m\pi/2B$, Φ_r is the sediment load function relative to the reference flow conditions, and $R=r\theta_r^{-1/2}/\beta_r$. Thanks to the linearity of the problem, the response of each Fourier component can be investigated independently of the others. The complete linear solution can be then reconstructed by superimposition. Each mode is a function of the position along the channel ($M=f(\xi)$), in a way similar to the problem of channels formation in alluvial fans recently tackled by Tambroni et al. (2019). Moreover, we observe that the effect of spatial width variations is felt at the spatial scale of bars through D_0 and U_0. Ultimately, it is the definition of the flow depth and of the longitudinal velocity at the leading order that distinguishes the estuarine from the coastal case.

4. Results

In this chapter, we illustrate the outcomes of the linear stability analysis described in chapter 3. As a first step, the basic state is computed analytically from system (Equations 14a–14c); then, we solved numerically the linear system (19a-d) by means of a predictor-corrector explicit finite difference scheme (Bhallamudi & Chaudry, 1991; MacCormack, 1969). At the starting point of the simulations, we employed an initial condition in the form of a uniform small random perturbation of the bed topography.

First, we present the results for the estuarine case. The reference (equilibrium) conditions can be uniquely defined once the Gauckler-Strickler coefficient (k_s^*) and the following set of three dimensionless parameters (β_u,θ_u,d_u) are prescribed, with $d_u=d*/D_u^*$ the relative roughness. Initially, it is instructive to separate the effect of channel convergence by considering a straight tidal estuary, where $B_u^*\equiv B_m^*$ (i.e., $L_c^*\to\infty$). As a consequence, $\hat{y}$ turns to coincide with y, and the lateral boundaries lose the spatial dependency from ξ. This configuration can be representative of an artificial channel in presence of embankments to prevent lateral erosion as encountered in many regulation works commonly employed in highly populated areas.

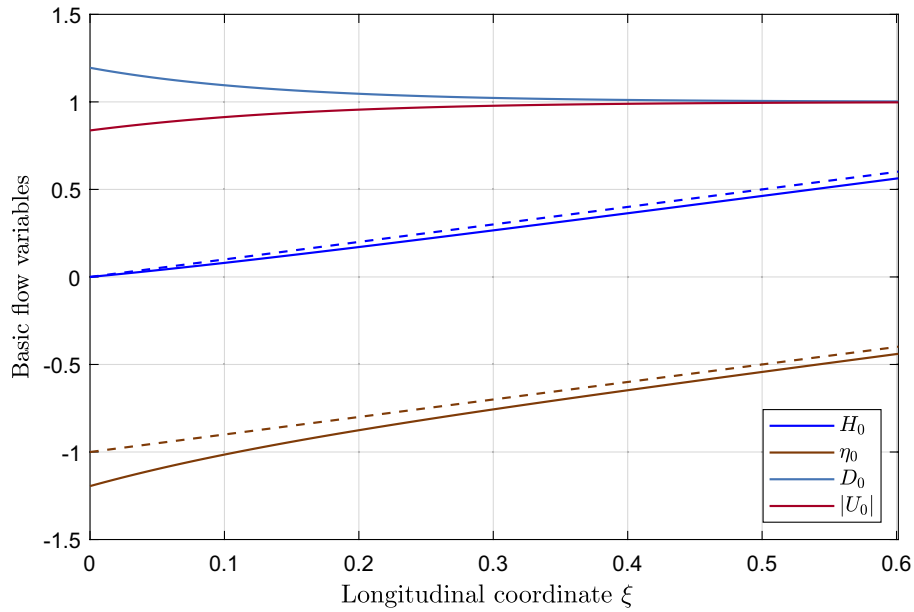

Figure 3. Equilibrium profiles of the governing variables (U_0, D_0, H_0, η_0) for a straight micro-tidal estuary, in terms of a given value of the scaled tidal amplitude (a). The bed elevation (η_0) is computed as the difference between the water surface elevation (H_0) and the flow depth (D_0). The tidal oscillation leads to a steeper bed slope as the sea is approached, with a consequent increase of D_0 and a reduction of the flow velocity $(|U_0|)$. The dashed lines stand for the solution of the water surface and bed elevation in the absence of tide (i.e., $a = 0$). The reference parameters are: $\beta_u = 10$, $\theta_u = 0.8$, $d_u = 0.001$, $a = 0.3$, and $k_s^* = 30\ \mathrm{m}^{1/3}\ \mathrm{s}^{-1}$.

In the example reported in Figure 3, profiles of the equilibrium variables are plotted in terms of the long spatial coordinate ξ for a given value of the scaled tidal amplitude. Due to the effect of the tidal forcing, a concave down bed profile $(\eta_0 = H_0 - D_0)$ develops, characterized by a steeper region at the mouth of the channel. The deepening at the inlet, which leads to a progressive reduction of the local aspect ratio, induces a slowdown of the river current (i.e., low values of the Shields number). For the set of parameters employed, uniform flow conditions (i.e., $|U_0| = D_0 = 1$) are recovered at $\xi \simeq 0.5$ or, in other words, when the length of the channel is a half of the backwater length L_b^*. We note that the upstream fluvial-dominated reach $(\xi > 0.5)$ is not directly affected by the tidal wave; this notwithstanding, the equilibrium bed elevation undergoes a gradual deepening with respect of the case when the tide is absent. Overall, the magnitude of the tide-induced scour is in the order of just a minor fraction of the uniform flow depth, ranging from about $0.2D_u^*$ at the mouth to $0.1D_u^*$ in the landward reach, as a consequence of the assumed small value of the dimensionless tidal amplitude.

The equilibrium condition reported in Figure 3 provides the basic state over which the disturbances are superimposed. Figure 4a shows the time evolution of the amplitude of the bed perturbations $(\mathcal{E}_1 = \mathcal{H}_1 - \mathcal{D}_1)$. A sequence of scours and deposits in the form of alternate bars slowly develops, amplifies, and migrates downstream leaving an unperturbed domain behind (see also Figure 4c). Several numerical and experimental works captured this latter behavior, formally proved by Federici and Seminara (2003), namely the observation that any local perturbation tends to be convected downstream rather than being spread throughout the whole channel (Defina, 2003; Fujita & Muramoto, 1985; Redolfi et al., 2020; Wu et al., 2011). Moreover, in the upstream part of the channel the rate of migration is in the order of 10 m per day, nearly halved in the seaward reaches. Not surprisingly, approaching the coast, bar growth and celerity are gradually damped. This is consistent with the well-known behavior arising from the fluvial bar theory (e.g., Tubino et al., 1999), whereby the growth rate of the fastest growing perturbation is an increasing function of the aspect ratio, which in turn decreases seaward in the present case. In Figures 4b and 4a, comparison between the evolution of $\mathcal{E}_1$ at three different locations along the channel as a function of the dimensionless time is shown. We note that, in spite of the modest deepening induced by the tidal wave, which in turn implies a small reduction of the local aspect ratio moving downstream, after nearly 60 tidal cycles the value of the bed

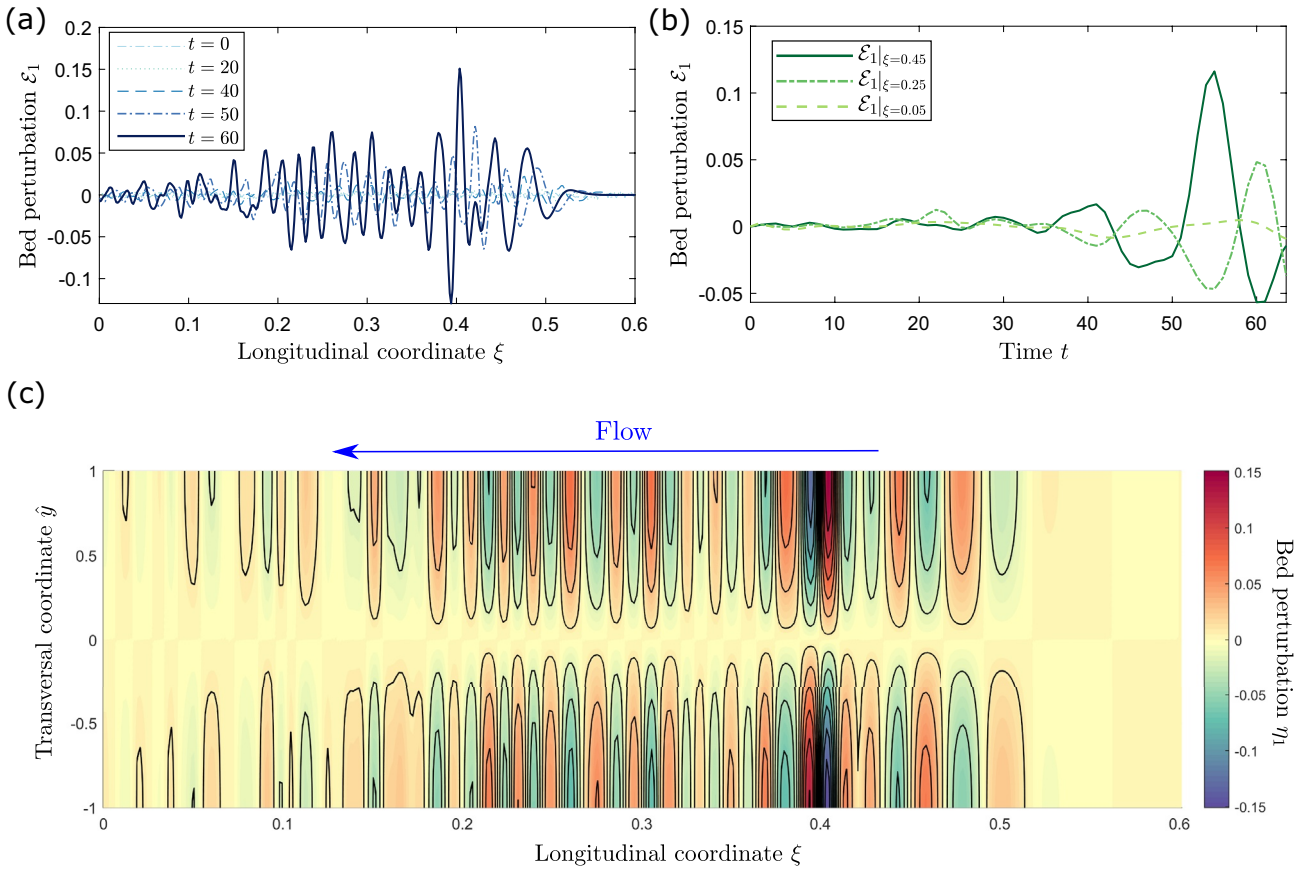

Figure 4. Evolution of the bed perturbation amplitude ($\mathcal{E}_1$) with respect to the equilibrium configuration reported in Figure 3 starting from random distributed disturbances assigned at $t = 0$. In panel (a), the spatial distribution of $\mathcal{E}_1$ is reported for different temporal instants; in panel (b), the temporal evolution of $\mathcal{E}_1$ is plotted at three different specified positions along the channel. Moving seawards, bar migration and amplification is progressively damped. Panel (c), the two-dimensional plot of the bed topography at $t = 60$. The reference parameters are: $\beta_u = 10$, $\theta_u = 0.8$, $d_u = 0.001$, $a = 0.3$, and $k_s^* = 30\ \mathrm{m}^{1/3}\ \mathrm{s}^{-1}$.

perturbations in proximity of the mouth are one order of magnitude lower than the ones in the upstream reaches. Furthermore, the plots indicate that in the seaward reach bars tend to lengthen. Nevertheless, differently from the growth rate, this effect is rather moderate, being the bar wavelength less sensible to a small variation of the reference parameters with values in the order of $10B_u^*$. Summarizing, tidal oscillations tend to prevent downstream migration of bars, along with a substantial reduction of the growth rate and a slightly increase of their wavelength.

We now relax the assumption on the straight planform shape of the estuary, by allowing width to vary in space according to Equation 1. To analyze the present case, we refer to a real-world micro-tidal estuary, the Magra River, Italy. The morphodynamic equilibrium of the terminal reach of the Magra River has been analyzed in detail by a recent work of Bolla Pittaluga et al. (2014). In Figure 5a, the basic state is reported, which shows a radically different picture with respect to the straight channel planform configuration: as width increases seaward, flow depth decreases along with the flow velocity to ensure flow and sediment mass conservation. This leads to channel shallowing toward the estuary mouth, which completely overwhelms the tide-induced scour. This result is not surprising, if we remind the structure of the solution of Seminara et al. (2012), where channel widening appears at the leading order, whereby river-tidal interactions appear just at successive orders of approximation (see Equations A1a–A1c). Nevertheless, we observe that to compensate the two opposing effects in terms of the tidal forcing, a value of a nearly equal to 0.6 (i.e., $a^* \simeq 1.5$ m) would be needed.

In Figure 6a, we report the temporal evolution of the maximum bed perturbation amplitude ($|\mathcal{E}_1|_{max}$), relatively to the first three lateral modes in the terminal widened reach corresponding to nearly the last 1500 m

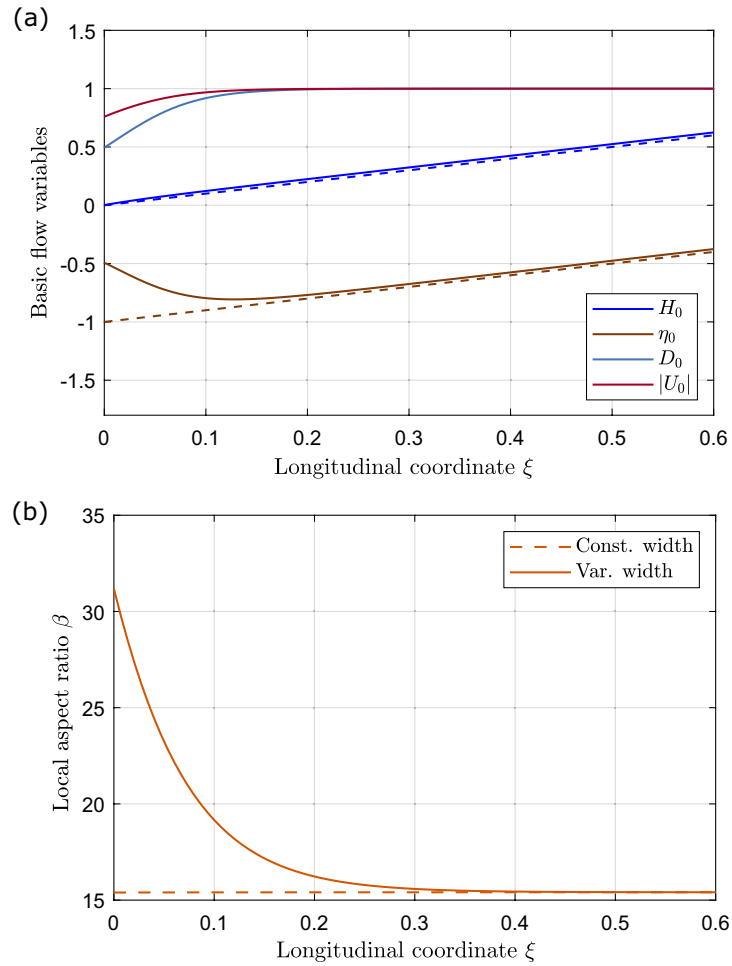

Figure 5. (a) Spatial distribution of the equilibrium variables for the Magra River estuary, showing the channel shallowing typical of diverging flows moving seaward. The dashed lines coincide with a straight fluvial channel in uniform flow conditions (i.e., $a = 0$, $B_m = 1$). In panel (b), it is reported the comparison between the local aspect ratio β for the converging profile (continuous line) and for an equivalent channel with a constant width equal to B_u^* taking into account the small tidal oscillation (dashed line). We note that in the constant width case, β is not equal to β_u, but slightly decreases toward the mouth due to the weak effect of the tide. Reference parameters are (see also Bolla Pittaluga et al., 2014): $\beta_u = 10.2$, $\theta_u = 0.39$, $d_u = 0.00017$, $a = 0.04$, and $k_s^* = 30\ \mathrm{m}^{1/3}\ \mathrm{s}^{-1}$.

of the estuary (i.e., $\xi \simeq 0.08$). The plot suggests that the linear theory selects the second mode (i.e., central bars) as the fastest growing mode, which displays an exponential growth after about 800 tidal cycles. In Figure 6b, the spatial evolution of the alternate and central bar mode, at a given time, is shown. Differently from Figure 6a, we extend the domain up to $\xi \simeq 0.18$ to show a peculiar feature: moving seawards, around $\xi \simeq 0.08$ there is a transition of the dominant mode, passing from alternate bars to central bars, due to channel shallowing that promotes bars formation with higher growth rates. Moreover, the linearity of the model allows to reconstruct the solution by superimposition, returning a complex bed topography as reported in the two-dimensional plot of Figure 6c.

The flow depth reduction in the widened reach leads to a sharp increase of the local value of the aspect ratio, as shown in Figure 5b. It is well known from river bar stability theories (e.g., Blondeaux & Seminara, 1985; Fredsøe, 1978; Parker, 1976) that large values of β promotes the development of multiple row bars (i.e., $m > 1$). We observe that, while β increases being a destabilizing factor, the local Shields number decreases trying to stabilize the system. However, the former parameter prevails in determining the bed instability. This can be understood by considering the Exner equation, and in particular, the transversal component of the sediment flux. In addition, the Exner equation provides a physical explanation of such instability, which

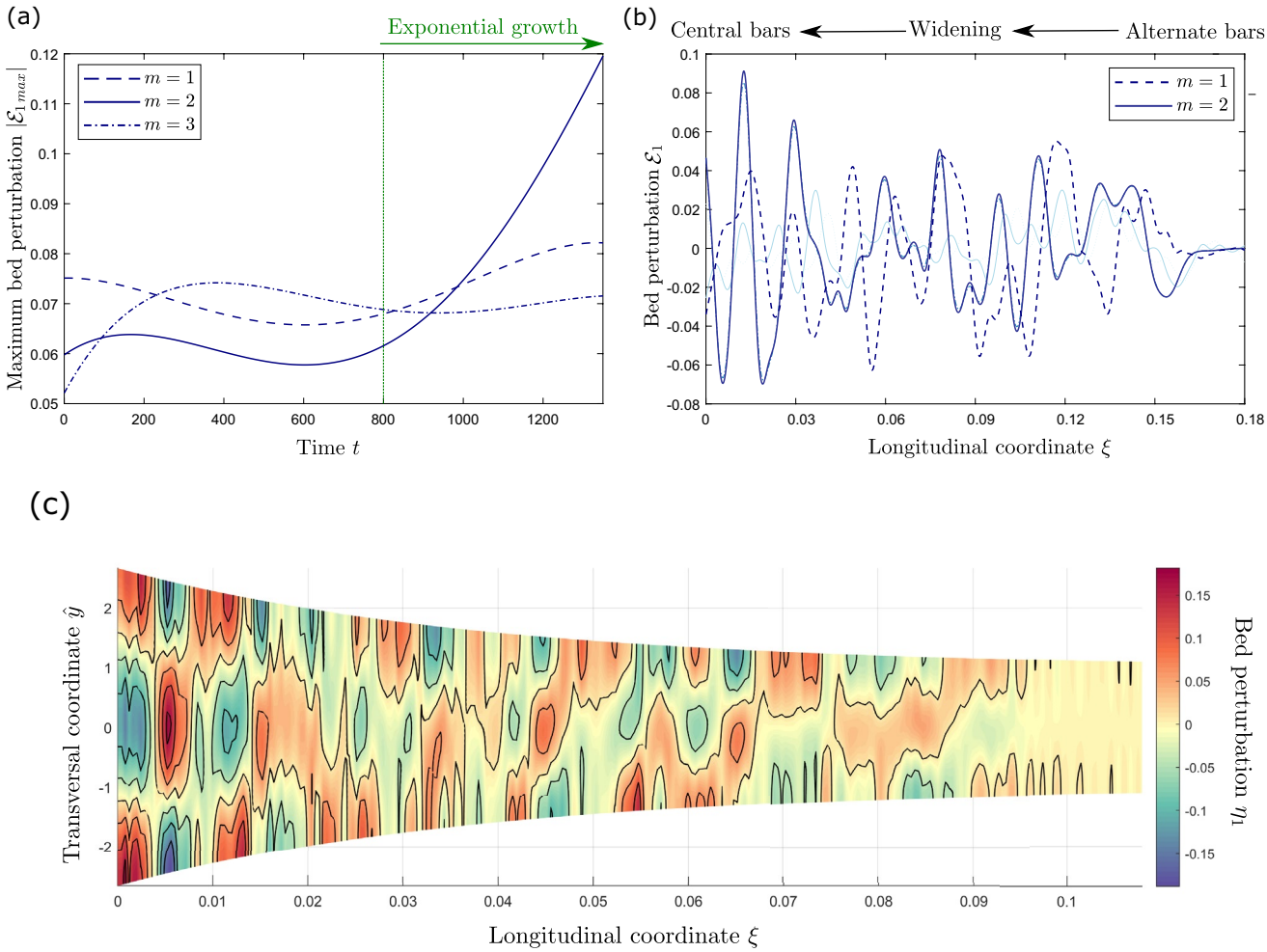

Figure 6. Evolution of the amplitude of the bed perturbations with respect to the equilibrium configuration of the Magra River reported in Figure 5a, starting from a random distributed disturbance. In panel (a), the temporal behavior of the maximum amplitude of the bed perturbations ($|\mathcal{E}_1|_{max}$) for the first three lateral modes in the widened reach. The most unstable mode is the one corresponding to central bars ($m = 2$). Panel (b) shows the spatial evolution of the first and second lateral mode at $t = 1200$ for the last 3000 m of the estuary ($0 \leq \xi \leq 0.18$). The shaded light-blue line on the background corresponds to the initial random perturbation. At nearly $\xi \simeq 0.08$ there is a transition of the dominating mode. Panel (c), the two-dimensional plot of the bed topography at $t = 1200$, where the bed perturbation η_1 has been re-constructed by superimposition of the first lateral two modes. Reference parameters are: $\beta_u = 10.2$, $\theta_u = 0.39$, $d_u = 0.00017$, $a = 0.04$, and $k_s^* = 30\ \mathrm{m}^{1/3}\ \mathrm{s}^{-1}$.

depends on the phase-lag between the response of the bed profile and the sediment transport. Specifically, instability is driven by a delicate balance between the destabilizing effect of the transverse shear stress (i.e., $\mathcal{V}_1$) and the stabilizing effect of the gravitational pull of sediment proportional to the transverse bed slope (see for a detailed explanation Colombini et al., 1987; Seminara & Tubino, 1989). We note that the latter term is proportional to m^2/β, hence it inhibits the development of higher-order modes.

We now proceed to investigate the case of tidal channels in which no freshwater and sediment discharges are supplied from upstream. The linear model is tested by performing a comparison with the results of the second experiment carried out in a funnel-shaped tidal channel and described by Tambroni et al. (2005) (see their Table 1 for the experimental data set). With reference to the longitudinal bed profile observed at different time steps during the experiment, as shown in Figure 7a, we consider three different bottom configurations: a plane bed (i.e., $D_0^{flat} = 1$) corresponding to the initial stage; two approximated linear bed profiles calibrated on the basis of the cross-sectional averaged bed topography reported by Tambroni et al. (2005) in their Figure 5 after 60 and 100 tidal cycles, respectively. Furthermore, in Figure 7a the final (asymptotic)

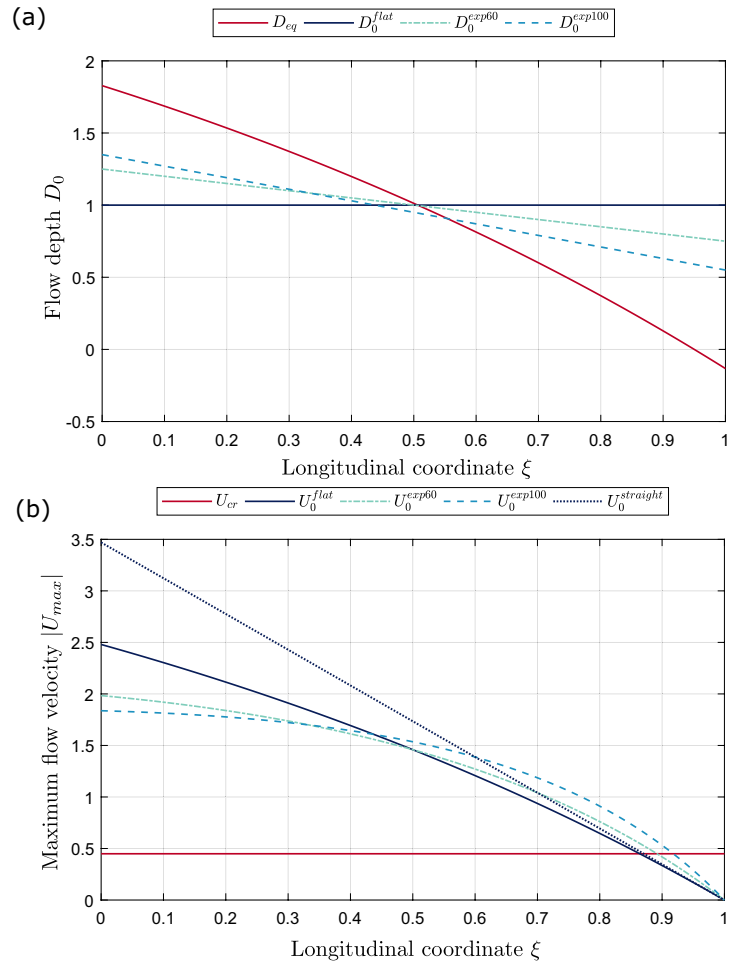

Figure 7. Leading-order (a) depth and (b) velocity profiles relatively to the second experiment performed in a funnel-shaped channel by Tambroni et al. (2005). The reported flow depth was obtained by linearly approximating the cross-sectional averaged bed profile observed in the experiment. The superscripts in the legend indicate the different time stages of the experimental performance, starting from $t^{exp} = 0$ (i.e., flat bed), till the final (asymptotic) equilibrium configuration, where the maximum flow velocity in a tidal cycle its equal to the maximum speed for sediment motion (U_{cr}^*). In panel (b), $U_0^{straight}$ is the peak flow velocity for a straight channel at $t^{exp} = 0$, with U_0 computed according to Equation 20.

equilibrium bed profile is reported, where the flow velocity corresponds to the critical velocity for the sediment motion U_{cr}^*, and can be computed as follows (Seminara et al., 2010):

$$D_{eq} = \frac{L_c^*}{L_\infty^*}\left\{1 - \exp\left[\frac{L_{eq}^*}{L_c^*}(\xi - 1)\right]\right\}, \tag{20a}$$

$$L_\infty^* = \frac{U_{cr}^*}{a\sigma^*}\left|\frac{df}{dt}\right|_{max}, \quad L_{eq}^* = -L_c^* \ln\left[1 - \frac{L_\infty^*}{L_c^*}\right], \tag{20b}$$

where L_{eq}^* and L_∞^* are the equilibrium length for a convergent and a straight channel, respectively. In Figure 7b, the maximum speed attained during a tidal cycle in each cross-section is illustrated concerning to the simple case of a single sinusoidal function (i.e., $f(t) = \sin(t)$). The basic flow field (U_0) is computed by means of Equation 15. The plot shows the tendency of U_0 to be spatially uniform as it progressively evolves toward its final equilibrium state with the exception of a close region toward the landward end, as observed numerically (e.g., Lanzoni & Seminara, 2002; Pritchard et al., 2002; Todeschini et al., 2008) and in field case studies (e.g., Friedrichs, 1995; Leopold et al., 1993). From the plot, it is also evident that during part of the tidal cycle the flow velocity is lower than the threshold for the sediment motion.

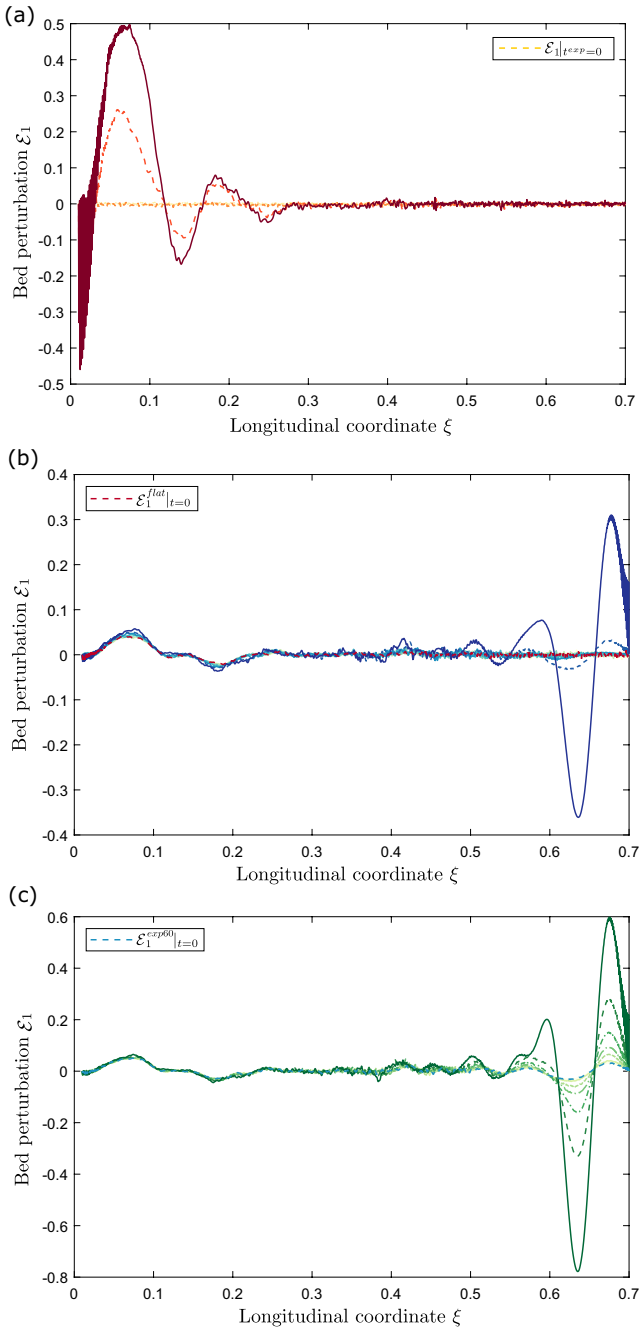

Figure 8. Spatial evolution of the amplitude of the bed perturbations with reference to the basic state reported in Figure 7, at subsequent time steps (indicated by the dashed lines with increasing darker colors). In panel (a), the flat bed of the channel ($\mathcal{E}_1|_{t^{exp}=0}$) is perturbed by a small random perturbation, which leads the formation of two long bars in the seaward reach of the channel. Subsequently, we employ the channel configuration of panel (a) ($\mathcal{E}_1^{exp60}|_{t=0}$), at an intermediate time step to perturb the basic state corresponding to the experimental time $t^{exp} = 60$ (red dashed line, panel b). Finally, in panel (c) we follow the same procedure to analyze the instability process at $t^{exp} = 100$, in which it appears how the initially formed bars near the mouth of the channel cease to grow. The bed is observed to lose its stability quite fast, nearly after one/two (simulated) tidal cycles in all the three configurations.

We then proceed to perturb the basic state by taking advantage of the different timescales that govern the undertaken problem; that is, we rely on the laboratory and numerical observations (see Tambroni et al., 2005; van der Wegen & Roelvink, 2008) that the longitudinal profile develops on a much slower timescale than the timescale governing the bars formation. Hence, the basic state D_0 at a given time can be considered as fixed. We consider first a flat bed (Figure 8a): the small, random perturbations coalesce and begin to grow in the form of two long waves at the mouth of the channel, where the peak velocity (i.e., the peak Shields number) is higher (see Figure 7b). In this initial stage, the peak value of the Shields parameter, which governs the intensity of the sediment transport, has a primary role. We remind that the latter, by means of the Engelund and Hansen (1967) formula, establishes a strong nonlinear dependency upon the flow velocity (i.e., $|\boldsymbol{q_s}| \propto |U|^5$).

We then proceed to the second phase. As initial condition, we perturbed the basic state associated with the bed profile D_0^{exp60} with the bed perturbation obtained from the plane bed simulation $\mathcal{E}_1^{flat}$, as shown in Figure 8b. A sequence of scours and deposits starts to grow in the landward part of the channel. In this region (from nearly $\xi \simeq 0.4$) the maximum value of the flow velocity increases with respect to the initial stages. Furthermore, the local value of the aspect ratio also increases due to channel shallowing, while at the same time, seaward reaches are characterized by lower values of the Shields number and of the aspect ratio, caused by a progressive channel deepening. However, the initially triggered bars still amplify, but with a slower growth rate. We note that any net migration is not observed, as clearly expected due to the symmetric tidal forcing imposed.

To investigate the third phase corresponding to the experimental conditions after 100 tidal cycles, we follow the same methodology previously described. The perturbations $\mathcal{E}_1^{exp60}$ are superimposed to the basic sloping bed D_0^{exp100}. Bars are observed to continuously grow landward, without significantly changing their wavelength. However, amplification in the seaward reach is almost completely ceased. Remarkably, results suggest that in this region characterized by a progressive channel deepening, bars formed in the initial stages of the channel evolution gradually grow till eventually achieving a frozen amplitude pattern where the pre-existing bars are not significantly varying in time and any newborn bar is observed to develop. The above findings are supported by the results of the laboratory experiments of Tambroni et al. (2005). We try to compare the wavelengths resulting from our linear model of Figure 8c with those observed by the latter authors. This choice is motivated from experimental observations in the fluvial context (e.g., Fujita & Muramoto, 1985), where the selection process of bar wavelength is relatively fast, and therefore, can be satisfactorily predicted in the context of a linear theory. On the other hand, linear theory does not allow for a direct comparison in the advanced phases of the experimental performances, where nonlinear interactions are expected to play a crucial role. As shown in Figure 9, the linear model seems to slightly overestimate the observed wavelength, being in the order of 3–6 channel widths. Finally, we observe that from experimental observations bars are observed to gradually adjust their length and height with an increasingly slower rate during the process of the bed evolution, an observation pointed out also by van der Wegen and Roelvink (2008) in their numerical investigation.

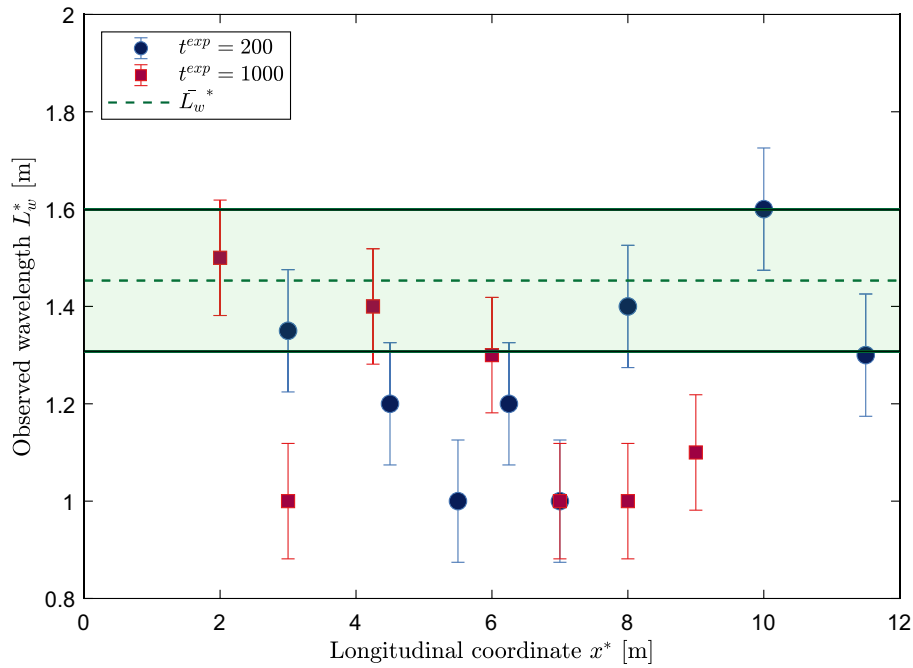

Figure 9. Comparison between the observed wavelengths in the experiment performed by Tambroni et al. (2005) after 200 and 1000 tidal cycles, and the mean predicted wavelength $\bar{L}_w^*$ by the linear model after 100 tidal cycles (see the bed topography reported in Figure 8c). The spacing between the solid lines corresponds to ± 10% of $\bar{L}_w^*$. The round and square markers represent the median values of the observed experimental wavelengths.

5. Discussion

In this paper, we propose a semi-analytical linear model to study the incipient formation of free bars in tidal environments. Differently from previously developed theoretical models, we account for the tide-induced seaward width expansion, as commonly encountered in natural tidal channels and estuaries. A novelty of the work is represented by the model proposed in chapter 2 that gathers in an unified mathematical framework both the transition of a river into a tidal sea characterized by small tidal oscillations with respect to the average flow depth (estuarine case), and the case of a short tidal channel in the absence of a fluvial supply of freshwater and sediment (coastal case). By assuming that the ratio between the spatial scale of bars and the scale of width variations is small, the problem can be tackled analytically without major complications.

In the context of a linear stability analysis, the main difference between the estuarine and the coastal case resides in the definition of the basic state upon which the analysis of the growth/decay of the superimposed infinitesimal perturbations is performed. In the former case, bars formation is interpreted as the outcome of an inherent instability of the (tidally averaged) equilibrium state. In the latter case, an (almost) vanishing net sediment flux condition distinguishes the equilibrium state of tide-dominated channels. Thus, the problem has to be faced from a different perspective. Specifically, we take advantage of the distinct temporal scales involved: modifications of the bed elevation can be regarded as high-frequency perturbations with respect to the timescale of bar instability and, naturally, of the hydrodynamic timescale (i.e., the tidal period). Hence, the basic flow field describes the propagation of a tidal wave with appropriate boundary conditions forced at the channel ends (see Equation 15), while the bed profile is a function of the spatial scale only at each instant of the tidal cycle and of the bars timescale.

Results reported in Figure 8 suggest that bars in tidal channels arise far from the equilibrium state of the system and, in the ideal absence of flow asymmetries and/or residual currents that prevents any net migration over a tidal cycle, they oscillate forward and backward in a symmetric fashion. In order to analyze the effect of (external) overtides, let us introduce a second harmonic as follows:

$$f(t) = \sin(t) + \alpha \sin(2t - \varphi), \tag{21}$$

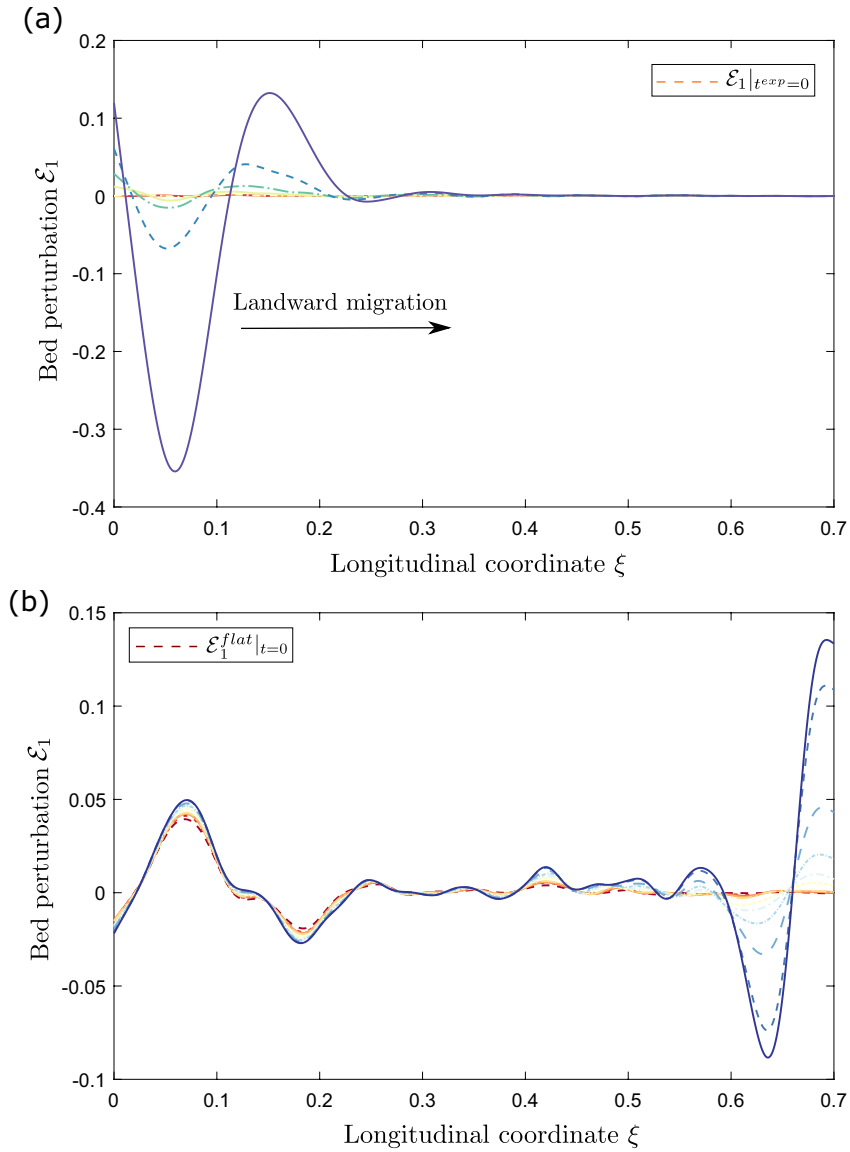

Figure 10. Spatial evolution of the bed perturbations in the (a) plane bed configuration, and (b) linear bed profile measured by Tambroni et al. (2005) after 60 tidal cycles. The dashed lines denote intermediate time steps. In turn, continuous lines correspond to the values of $\mathcal{E}_1$ after two (simulated) tidal cycles, where the simulation stops to prevent the infinite growth of the instabilities. The perturbation of the basic state is performed following the same procedure described in Figure 8. However, differently from Figure 8, the boundary condition at the mouth consists of a secondary harmonic with amplitude $\alpha = 0.2$ and a relative phase-lag $\varphi = 0$, chosen in such way to generate a flood-dominated flow field (see Equation 21), which induces a slow landward migration of the bars.

where α is the scaled amplitude of the second harmonic, and φ is the related phase-lag. We perform some simulations, whose outputs are reported in Figure 10, relatively to a flood dominance ($\varphi = 0$), namely the fact that the flood peak velocity is higher than its ebb value. Consequently, a net bar motion is observed, in the order of $\xi \simeq 10^{-2}$ in a tidal cycle, corresponding to a net migration $\Delta x \simeq 10^{-1}$ channel widths, a value comparable with those obtained by the modeling study of Garotta et al. (2006) (see their Figure 16). It is worthwhile to observe that the overall behavior of the instability process is unchanged with respect to the single-harmonic case. Specifically, in the first temporal stages, just the seaward part of the channel is observed to lose its stability to the oscillatory tidal wave (see Figure 10a), whereas the rest of the channel remains flat. On the contrary, as the channel evolves and the flow field adapts to this slow variation, bed perturbations in other parts of the channel, in particular the landward reaches, start to amplify. In this sense,

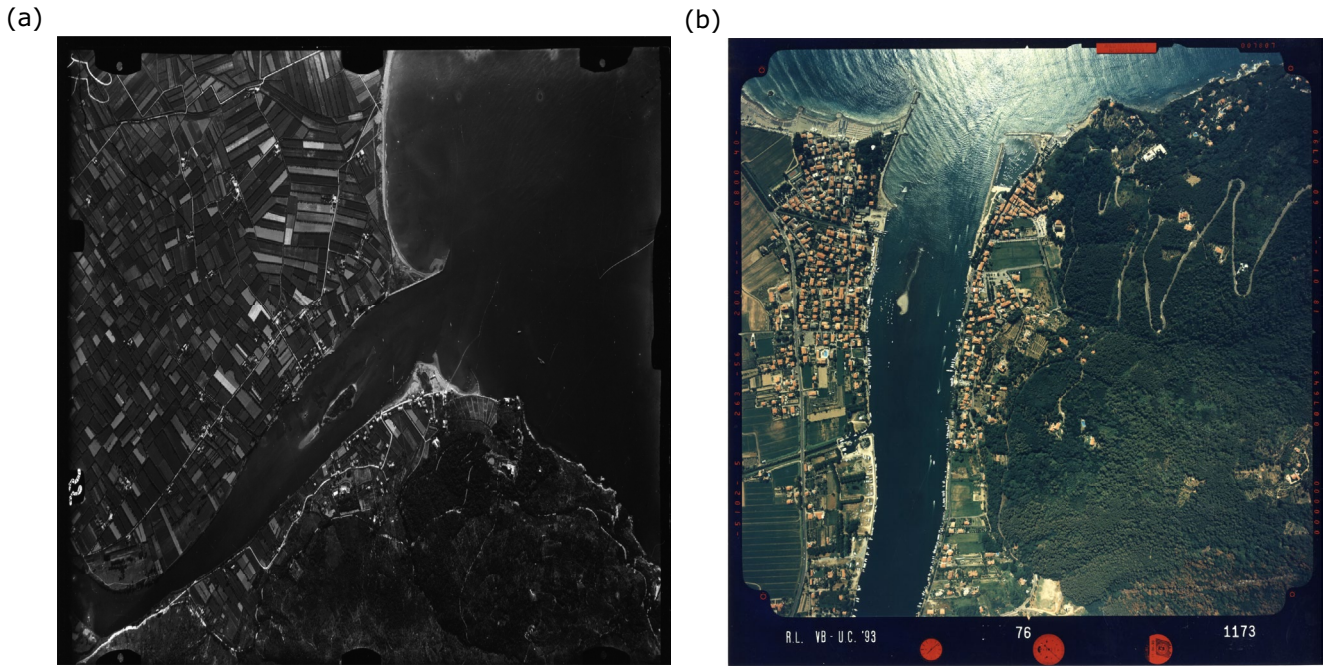

Figure 11. Historical aerial photographs of the Magra River estuary in the (a) 1937 and (b) 1993. An emerged island is clearly visible near the mouth of the estuary. The photographs are publicly available at https://geoportal.regione.liguria.it/.

Figure 10b shows that any newborn bar is not observed in the seaward reach, in which the "old" triggered perturbations just continue to grow. Unfortunately, an interpretation in the light of the work of Tambroni et al. (2005) is difficult because the natural presence of a background "noise" in the experimental tests might give rise to repeated new disturbances.

Tidal bars crucially reflect the initial conditions. Considering an initial condition in the form of a linearized bottom topography, as commonly employed in numerical modeling (e.g., Hibma et al., 2003; van de Lageweg & Feldman, 2018; van der Wegen & Roelvink, 2008), might have sensible consequences for the model outcomes and their relative interpretation. In particular, the majority of these works highlights that tidal bars start to form in the landward part of the channel. In this region of the domain the local aspect ratio, which has a primary role in the instability process as we have seen so far, is higher than in the seaward reach. Consequently, we could foresee that, according to the linear theory, bars grow faster in the shallow part of the channel. On the other hand, a different behavior might be expected if simulations are carried out starting from a flat bed (i.e., the initial channel aspect ratio is spatially uniform). Indeed, this is what emerges from the linear model as shown in Figures 8 and Figure 10, where bars start to form near the mouth of the tidal channel due to the higher flow velocity in that zone (i.e., higher sediment flux).

We now look at the estuarine case. Here, under suitable circumstances bars arise due to an instability of the equilibrium state. For the straight estuary analyzed in Figure 4, tidal currents, which tend to reduce the bar growth and migration rate, yet are not necessarily strong to prevent bars amplification. However, we might expect that for particularly straight and deep channels close to the critical conditions, even modest tidal amplitudes may be sufficient to prevent bars formation approaching the coastline. In the case of a real funnel-shaped estuary like the Magra River, the seaward width expansion leads to channel shallowing, hence, a progressive increase of the channel aspect ratio, which have a destabilizing effect. The latter factor is observed to overwhelm the stabilizing scouring effect performed by the tides, leading higher order lateral modes (i.e., midchannel and/or multiple row bars) to be the most unstable ones. In other words, the linear analysis suggests that for a set of reference parameters several types of bars might be present in different portions of the channel (see Figure 6b), whereas their competition can be studied only with a nonlinear model.

The linear analysis suggests that midchannel bars are expected in the Magra River estuary. Indeed, historical aerial photographs of the Magra River from the 1937 (Figure 11a) and 1993 (Figure 11b), show that an exposed island was present in the estuary. In the last decades, arguably due to the recurrent dredging activities and other anthropic interventions, the island is no longer visible. Nevertheless, it is interesting to observe that the island appeared to be a steady feature. An interpretation in the light of the present model is not straightforward: the selected perturbations from the stability analysis are migrating patterns (see Figure 6b). This latter characteristic hides a more substantial implication than it might appear at a first sight, being closely tied with the nature of the proposed linear model. Specifically, at the linear level, the forcing effect exerted by width variations (i.e., $\propto \gamma$) does not affect the boundary conditions, thus, the eventual interaction of free bars with forced bars triggered by the geometrical variations is herein not captured, by the fact that the latter act on the slow spatial scale ξ. In turn, this interaction may lead to suppression of migrating free bars in favor of stationary forced bars in a similar fashion as the mechanism observed in river meanders (Kinoshita & Miwa, 1974; Seminara & Tubino, 1989; Tubino & Seminara, 1990).

Let us discuss the main limitations of our work. In this paper, we developed a theoretical framework, which due to its intrinsic linear nature prevents the possibility to predict an equilibrium bar amplitude. Nonlinear interactions between the flow field and the (slowly) evolving bottom topography, become significant as the amplitude of the perturbations grows. As the channel bed moves toward its equilibrium condition, also the geometrical characteristics of the growing modes modify. In particular, longer bedforms are observed (Hibma et al., 2003; van der Wegen & Roelvink, 2008). A nonlinear formulation would allow to directly address how bars reflect the history of the system in its approach toward the equilibrium, and to study the possible coexistence and interaction between free and forced bars, which still awaits to be investigated. More in general, forced bars in tidal channels received a less much attention, where just a few studies have tried to give a mechanistic explanation to the development of point bars in tidal meanders (Solari et al., 2002; Tambroni et al., 2017), while Leuven et al. (2018) performed several experiments to analyze the planimetric effect of growing forced bars due to width variations in self-formed estuaries.

We adopted a total load formula to quantify the sediment transport. We believe that for the purposes of this work, this assumption does not change qualitatively our results. Nevertheless, we remind that with the employment of the Engelund and Hansen (1967) predictor we implicitly ignore that the gravitational correction necessary to determine the direction of the sediment flux vector (see Equation 11b) strictly applies only to the bedload component. Modeling transport in suspension will require the solution of a convection-diffusion equation. Furthermore, it has been observed that the presence of a significant contribution of the suspended load tends to give rise to longer bedforms, especially when the bed is composed by very fine sand and exposed to strong tidal currents (e.g., Blondeaux & Vittori, 2009; Seminara & Tubino, 2001).

The effect of tidal flats, which is known (see Seminara et al., 2010) to lead to flow acceleration in the channel and, as a result, a shorter equilibrium length, has been neglected. We believe that the future inclusion of this factor may be particularly relevant for tide-dominated channels. Moreover, the assumption on the fixed channel banks is less stringent. Banks in tidal channels are typically characterized by an higher erosion resistance with respect of their fluvial counterpart, due to sediment autocompaction, stabilization provided by halophytic vegetation especially in salt marshes, and a more homogeneous substrate (Finotello et al., 2020; Garofalo, 1980; Kleinhans et al., 2009; Solari et al., 2002). We note that the potential erosion induced by wind waves has been disregarded. Finally, we have considered a bed characterized by a homogeneous sediment composition. Relaxing this assumption will allow to explore the role of sorting process in the growth of tidal bars (Van Oyen & Blondeaux, 2009; Viparelli et al., 2019).

6. Conclusions

In this work, we propose a general theoretical framework that is able to describe the incipient phase of bars development in a wide range of environmental settings where variations of the physical boundaries (i.e., channel width, tide-induced flow depth) are smooth, acting on a spatial scale that is much longer than bars wavelength. On the basis of the model formulation and subsequent analysis, we can draw the following conclusions:

1. Bars formation in micro-tidal estuaries (estuarine case) and tidal channels (coastal case) can be studied within a unified linear model once the boundary conditions of the problem and a reference flow, which represents the basic state upon which small amplitude disturbances are superimposed, are properly defined. The basic state requires the solution of a differential problem that can be solved analytically by means of perturbation techniques, allowing for deep insights in the physical mechanisms controlling the dynamics of the system.
2. In the estuarine case, where bars arise from an instability of the equilibrium state, the erosive character of the tidal motion and the channel shallowing induced by the increase in width moving seawards, are two opposite factors that concur to affect bars formation and properties (i.e., growth rate, celerity, and in lesser extent, wavelength). However, in micro-tidal conditions, the tide-induced scour is typically one-order of magnitude smaller than the drop of depth induced by the flow expansion, which in turn leads to higher values of the channel aspect ratio promoting the development of multiple row bars.
3. Bars in tidal channels form far from the final equilibrium state of the system and, in the ideal absence of mean residual currents and overtides, they oscillate forward and backward in a symmetric fashion. In the first temporal stages of the channel evolution, when the longitudinal bed profile is nearly flat, bars are observed to form just near the inlet. However, as the channel evolves, bars start to grow landward due to a progressive channel shallowing. At the same time, bars formed in the initial stages continue to grow yet with gradually slower growth rates, till eventually achieving a frozen amplitude pattern, where any newborn bar is observed to develop in the seaward reach. Consequently, the model indicates that the spatial-temporal distribution and properties of bars observed in nature reflects the (long-term) evolution history of the channel.
4. This work provides a simple, theoretically based, modeling framework that can be used to interpret results from physical experiments and numerical or field data, with the key advantage to require a relatively small computational effort.

Appendix A: Morphodynamic Equilibrium of a Micro-Tidal Estuary

In this section, we provide the analytical solution as obtained by Seminara et al. (2012) by means of a perturbation approach relatively to the tidally averaged morphodynamic equilibrium in the estuarine case. If we consider monochromatic tidal waves (i.e., $f(t) = \sin(t)$), neglecting the possible presence of externally generated overtides (Aubrey, 1986), the up to order a^2 form of the tidally averaged longitudinal distribution of the flow depth D_0, free surface elevation H_0, and fluid discharge q_0 for an estuary at equilibrium, reads (Seminara et al., 2012):

$$q_0 = -\frac{\delta}{\delta + \exp(-\psi\xi)}, \tag{A1a}$$

$$D_0 = |q_0|^{\frac{8}{11}} + a^2\Gamma\exp[-2\Re(\zeta)\xi], \tag{A1b}$$

$$H_0 = \int_0^{\xi} q_0(s)^{-\frac{14}{33}} ds + a\frac{F_u^2}{2}\left[\left(\frac{\delta}{\delta+1}\right)^{6/11} - \left(\frac{\delta}{\delta+\exp(-\psi\xi)}\right)^{6/11}\right] + a^2\int_0^{\xi}\Xi\exp[-2\Re(\zeta)s]ds, \tag{A1c}$$

with:

$$\delta = \frac{1}{B_m - 1}, \qquad \psi = \frac{D_u^*}{SL_c^*} = \frac{L_b^*}{L_c^*}, \tag{A2}$$

where B_m is the scaled width at the mouth. The ζ coefficient, which comes from the time-dependent part of the first-order expansion, reads as follows:

$$\zeta = \frac{1}{2}\left(k_1 + \sqrt{k_1^2 - 4k_2}\right), \tag{A3a}$$

$$k_1 = \mathcal{B} + \frac{10}{3}|q_0|^{-38/33}, \quad k_2 = \frac{d\mathcal{B}}{d\xi} + \frac{10}{3}|q_0|^{-38/33} - 2i\mu|q_0|^{-47/33}, \tag{A3b}$$

with μ and $\mathcal{B}$ a measure of the effect of local inertia relative to convective transport and relative rate of width reduction, respectively:

$$\mu = \frac{\sigma^* L_b^*}{U_u^*}, \qquad \mathcal{B} = -\psi \frac{e^{-\psi\xi}}{\delta + e^{-\psi\xi}}. \tag{A4}$$

Finally, the coefficients Γ and Ξ enclosing the nonlinear interactions between the zero-order and first-order part of the solution, are obtained by performing a tidal average. They read:

$$\Gamma = \left[\frac{13}{8}|q_0|^{-8/11}(|\zeta|^2 + \mathcal{B}^2 - 2\zeta\mathcal{B}) + \frac{5}{4}\frac{i\mu}{|q_0|}(\mathcal{B} - \mu) - \frac{10}{11}|q_0|^{-14/11}\mu^2\right]\frac{1}{\mathcal{B}|^2_{\xi=0}+|\zeta|^2 - 2\zeta\mathcal{B}|_{\xi=0}}, \tag{A5a}$$

$$\Xi = \left[-\frac{65}{36}|q_0|^{-62/33}(|\zeta|^2 + \mathcal{B}^2 - 2\zeta\mathcal{B}) - \frac{5}{2}\frac{i\mu}{|q_0|^{71/33}}(\mathcal{B} - \mu) - \frac{167}{66}|q_0|^{-80/33}\mu^2\right]\frac{1}{\mathcal{B}\,|^2_{\xi=0}+|\zeta|^2 - 2\zeta\mathcal{B}|_{\xi=0}}. \tag{A5b}$$

Data Availability Statement

A Matlab code that numerically solves the problem for a weakly converging micro-tidal estuary by means of the MacCormack scheme is made available in a public repository at https://doi.org/10.5281/zenodo.4659756.

Acknowledgments
The work has highly benefited from the thoughtful comments of the Editor A. J. F. Hoitink, the Associate Editor, and three anonymous reviewers. Open Access Funding provided by Universita degli Studi di Genova within the CRUI-CARE Agreement.

References

Adami, L., Bertoldi, W., & Zolezzi, G. (2016). Multidecadal dynamics of alternate bars in the Alpine Rhine River. *Water Resources Research*, *52*(11), 8938–8955. https://doi.org/10.1002/2015wr018228

Aubrey, D. G. (1986). Hydrodynamic controls on sediment transport in well-mixed bays and estuaries. In J. van de Kreeke, (Ed.) *Physics of shallow estuaries and bays* (pp. 245–258). New York, NY: Springer-Verlag. https://doi.org/10.1029/ln016p0245

Bertagni, M. B., & Camporeale, C. (2018). Finite amplitude of free alternate bars with suspended load. *Water Resources Research*, *54*(12), 9759–9773. https://doi.org/10.1029/2018wr022819

Bhallamudi, S. M., & Chaudry, M. H. (1991). Numerical modeling of aggradation and degradation in alluvial channels. *Journal of Hydraulic Engineering*, *117*(9), 1145–1164. https://doi.org/10.1061/(asce)0733-9429(1991)117:9(1145)

Bittner, L. (1995). *River bed response to channel width variation: Theory and experiments, Master thesis*. University of Illinois.

Blondeaux, P., & Seminara, G. (1985). A unified bar-bend theory of river meanders. *Journal of Fluid Mechanics*, *157*, 449–470. https://doi.org/10.1017/S0022112085002440

Blondeaux, P., & Vittori, G. (2009). The formation of tidal sand waves: Steady versus unsteady approaches. *Journal of Hydraulic Research*, *47*(2), 213–222. https://doi.org/10.3826/jhr.2009.3295

Blondeaux, P., & Vittori, G. (2011). Dunes and alternate bars in tidal channels. *Journal of Fluid Mechanics*, *670*, 558–580. https://doi.org/10.1017/S0022112010005458

Bolla Pittaluga, M., Luchi, R., & Seminara, G. (2014). On the equilibrium profile of river beds. *Journal of Geophysical Research: Earth Surface*, *119*(2), 317–332. https://doi.org/10.1002/2013jf002806

Bolla Pittaluga, M., Tambroni, N., Canestrelli, A., Slingerland, R., Lanzoni, S., & Seminara, G. (2015). Where river and tide meet: The morphodynamic equilibrium of alluvial estuaries. *Journal of Geophysical Research: Earth Surface*, *120*, 75–94. https://doi.org/10.1002/2014jf003233

Callander, R. A. (1969). Instability and river channels. *Journal of Fluid Mechanics*, *36*(3), 465–480. https://doi.org/10.1017/S0022112069001765

Chatanantavet, P., Lamb, M. P., & Nittrouer, J. A. (2012). Backwater controls of avulsion location on deltas. *Geophysical Research Letters*, *39*(1), L01402. https://doi.org/10.1029/2011GL050197

Colombini, M., Seminara, G., & Tubino, M. (1987). Finite-amplitude alternate bars. *Journal of Fluid Mechanics*, *181*, 213–232. https://doi.org/10.1017/S0022112087002064

Colombini, M., & Tubino, M. (1991). Finite amplitude free-bars: A fully nonlinear spectral solution. In R. Soulsby, R. Bettes, February, & euromech (Eds.), *Sand transport in rivers, estuaries and the sea* (2 ed., pp. 163–169). Rotterdam: Balkema.

Cordier, F., Tassi, P., Claude, N., Crosato, A., Rodrigues, S., & Pham Van Bang, D. (2019). Numerical study of alternate bars in alluvial channels with nonuniform sediment. *Water Resources Research*, *55*(4), 2976–3003. https://doi.org/10.1029/2017WR022420

Dalrymple, R. W., & Choi, K. (2007). Morphologic and facies trends through the fluvial-marine transition in tide-dominated depositional systems: A schematic framework for environmental and sequence-stratigraphic interpretation. *Earth-Science Reviews*, *81*(3–4), 135–174. https://doi.org/10.1016/j.earscirev.2006.10.002

Dalrymple, R. W., & Rhodes, R. N. (1995). Estuarine dunes and bars. In G. M. Perillo (Ed.), *Geomorphology and sedimentology of estuaries*. Developments in sedimentology (pp. 359–422). Elsevier Science B.V. https://doi.org/10.1016/S0070-4571(05)80033-0

Davies, G., & Woodroffe, C. D. (2010). Tidal estuary width convergence: Theory and form in North Australian estuaries. *Earth Surface Processes and Landforms*, *35*(7), 737–n. https://doi.org/10.1002/esp.1864

de Swart, H. E., & Zimmerman, J. (2009). Morphodynamics of tidal inlet systems. *Annual Review of Fluid Mechanics*, *41*(1), 203–229. https://doi.org/10.1146/annurev.fluid.010908.165159

Defina, A. (2003). Numerical experiments on bar growth. *Water Resources Research*, *39*(4), 1–12. https://doi.org/10.1029/2002WR001455

Duró, G., Crosato, A., & Tassi, P. (2016). Numerical study on river bar response to spatial variations of channel width. *Advances in Water Resources*, *93*, 21–38. https://doi.org/10.1016/j.advwatres.2015.10.003

Eekhout, J. P., Hoitink, A. J., & Mosselman, E. (2013). Field experiment on alternate bar development in a straight sand-bed stream. *Water Resources Research*, *49*(12), 8357–8369. https://doi.org/10.1002/2013WR014259

Einstein, H. A. (1950). *The bed-load function for sediment transportation in open channel flows. Tech. Bulletin No., 126* (p. 71). U.S. Department of Agriculture.
Engelund, F. (1981). *The motion of sediment particles on an inclined bed. Progress Rep, 53* (pp. 15–20).
Engelund, F., & Hansen, E. (1967). *A monograph on sediment transport in alluvial streams* (p. 62). Copenhagen K: Technical University of Denmark 0stervoldgade.
Federici, B., & Seminara, G. (2003). On the convective nature of bar instability. *Journal of Fluid Mechanics*, *487*, 125–145. https://doi.org/10.1017/S0022112003004737
Fernandes, A. M., Törnqvist, T. E., Straub, K. M., & Mohrig, D. (2016). Connecting the backwater hydraulics of coastal rivers to fluviodeltaic sedimentology and stratigraphy. *Geology*, *44*(12), 979–982. https://doi.org/10.1130/G37965.1
Finotello, A., D'Alpaos, A., Bogoni, M., Ghinassi, M., & Lanzoni, S. (2020). Remotely-sensed planform morphologies reveal fluvial and tidal nature of meandering channels. *Scientific Reports*, *10*(1), 1–13. https://doi.org/10.1038/s41598-019-56992-w
Fredsøe, J. (1978). Meandering and braiding of rivers. *Journal of Fluid Mechanics*, *84*(4), 609–624. https://doi.org/10.1017/S0022112078000373
Friedrichs, C. T. (1995). Stability shear stress and equilibrium cross-sectional geometry of sheltered tidal channels. *Journal of Coastal Research*, *11*(4), 1062–1074
Friedrichs, C. T., & Aubrey, D. G. (1994). Tidal propagation in strongly convergent channels. *Journal of Geophysical Research*, *99*(C2), 3321–3336. https://doi.org/10.1029/93JC03219
Friedrichs, C. T., & Aubrey, D. G. (1996). Uniform bottom shear stress and equilibrium hypsometry of intertidal flats. In C. Pattiaratchi (Ed.), *Mixing in estuaries and coastal seas* (pp. 405–429). American Geophysical Union. https://doi.org/10.1029/ce050p0405
Fujita, Y., & Muramoto, Y. (1985). Studies on the process of development of alternate bars. *Bulletin of the Disaster Prevention Research Institute*, *35*(3), 55–86
Garofalo, D. (1980). The influence of wetland vegetation on tidal stream channel migration and morphology. *Estuaries*, *3*(4), 258–270. https://doi.org/10.2307/1352081
Garotta, V., Bolla Pittaluga, M., & Seminara, G. (2006). On the migration of tidal free bars. *Physics of Fluids*, *18*(9), 096601. https://doi.org/10.1063/1.2221346
Guo, L., van der Wegen, M., Roelvink, D. J., & Quing, H. (2014). The role of river flow and tidal asymmetry on 1-D estuarine morphodynamics. *Journal of Geophysical Research: Earth Surface*, *119*, 2315–2334. https://doi.org/10.1002/2014JF003110
Guo, L., van der Wegen, M., Roelvink, D. J., Wang, Z. B., & He, Q. (2015). Long-term, process-based morphodynamic modeling of a fluvio-deltaic system, part I: The role of river discharge. *Continental Shelf Research*, *109*, 95–111. https://doi.org/10.1016/j.csr.2015.09.002
Hall, P. (2005). On the non-parallel instability of sediment-carrying channels of slowly varying width. *Journal of Fluid Mechanics*, *529*, 1–32. https://doi.org/10.1017/S0022112004002794
Hepkema, T. M., de Swart, H. E., & Schuttelaars, H. M. (2019). Sensitivity of tidal bar wavelength to channel width. *Journal of Geophysical Research: Earth Surface*, *124*(10), 2417–2436. https://doi.org/10.1029/2019JF005032
Hibma, A., De Vriend, H. J., & Stive, M. J. (2003). Numerical modelling of shoal pattern formation in well-mixed elongated estuaries. *Estuarine, Coastal and Shelf Science*, *57*(5–6), 981–991. https://doi.org/10.1016/S0272-7714(03)00004-0
Hibma, A., Schuttelaars, H. M., & de Vriend, H. J. (2004). Initial formation and long-term evolution of channel-shoal patterns. *Continental Shelf Research*, *24*(15), 1637–1650. https://doi.org/10.1016/j.csr.2004.05.003
Jaeggi, M. N. R. (1984). Formation and effects of alternate bars. *Journal of Hydraulic Engineering*, *110*(2), 142–156. https://doi.org/10.1061/(asce)0733-9429(1984)110:2(142)
Jerolmack, D. J. (2009). Conceptual framework for assessing the response of delta channel networks to Holocene sea level rise. *Quaternary Science Reviews*, *28*(17–18), 1786–1800. https://doi.org/10.1016/j.quascirev.2009.02.015
Kinoshita, R., & Miwa, H. (1974). River channel formation which prevents downstream movement of transverse bars. *Shinsabo*, *94*, 12–17.
Kleinhans, M. G., Schuurman, F., Bakx, W., & Markies, H. (2009). Meandering channel dynamics in highly cohesive sediment on an intertidal mud flat in the Westerschelde estuary, the Netherlands. *Geomorphology*, *105*(3–4), 261–276. https://doi.org/10.1016/j.geomorph.2008.10.005
Langbein, W. B. (1963). The hydraulic geometry of a shallow estuary. *Bulletin of the International Association of Scientific Hydrology*, *8*(3), 84–94. https://doi.org/10.1080/02626666309493340
Lanzoni, S. (2000). Experiments on bar formation in a straight flume 1. Uniform sediment. *Water Resources Research*, *36*(11), 3337–3349. https://doi.org/10.1029/2000WR900160
Lanzoni, S., & D'Alpaos, A. (2015). On funneling of tidal channels. *Journal of Geophysical Research: Earth Surface*, *120*(3), 433–452. https://doi.org/10.1002/2014JF003203
Lanzoni, S., & Seminara, G. (1998). On tide propagation in convergent estuaries. *Journal of Geophysical Research*, *103*(1), 793–30812. https://doi.org/10.1029/1998JC900015
Lanzoni, S., & Seminara, G. (2002). Long-term evolution and morphodynamic equilibrium of tidal channels. *Journal of Geophysical Research*, *107*(C1). https://doi.org/10.1029/2000jc000468
Leopold, L. B., Collins, J. N., & Collins, L. M. (1993). Hydrology of some tidal channels in estuarine marshland near San Francisco. *Catena*, *20*, 469–493. https://doi.org/10.1016/0341-8162(93)90043-o
Leuven, J. R., Braat, L., van Dijk, W. M., de Haas, T., van Onselen, E. P., Ruessink, B. G., & Kleinhans, M. G. (2018). Growing forced bars determine nonideal estuary planform. *Journal of Geophysical Research: Earth Surface*, *123*(11), 2971–2992. https://doi.org/10.1029/2018jf004718
Lewin, J. (1976). Initiation of bed forms and meanders in coarse-grained sediment. *Bulletin of the Geological Society of America*, *87*, 281–285. https://doi.org/10.1130/0016-7606(1976)87<281:iobfam>2.0.co;2
Luchi, R., Zolezzi, G., & Tubino, M. (2011). Bend theory of river meanders with spatial width variations. *Journal of Fluid Mechanics*, *681*, 311–339. https://doi.org/10.1017/jfm.2011.200
MacCormack, R. W. (1969). The effect of viscosity in hypervelocity impact cratering. *Journal of Spacecraft and Rockets*, *69*(354). https://doi.org/10.2514/2.6901
Marani, M., Lanzoni, S., Zandolin, D., Seminara, G., & Rinaldo, A. (2002). Tidal meanders. *Water Resources Research*, *38*(11), 7–14. https://doi.org/10.1029/2001wr000404
Monegaglia, F., Tubino, M., & Zolezzi, G. (2019). Interaction between curvature-driven width oscillations and channel curvature in evolving meander bends. *Journal of Fluid Mechanics*, *876*, 985–1017. https://doi.org/10.1017/jfm.2019.574
Nienhuis, J. H., Hoitink, A. J., & Törnqvist, T. E. (2018). Future change to tide-influenced deltas. *Geophysical Research Letters*, *45*(8), 3499–3507. https://doi.org/10.1029/2018gl077638

Olesen, K. W. (1983). *Alternate bars in and meandering of alluvial river, Tech. rep*. Delft University of Technology.
Paola, C., & Mohrig, D. (1996). Palaeohydraulics revisited: Palaeoslope estimation in coarse-grained braided rivers. *Basin Research*, *8*, 243–254. https://doi.org/10.1046/j.1365-2117.1996.00253.x
Parker, G. (1976). On the cause and characteristic scales of meandering and braiding in rivers. *Journal of Fluid Mechanics*, *76*(3), 457–480. https://doi.org/10.1017/s0022112076000748
Parker, G. (1984). Lateral bed load transport on side slopes. *Journal of Hydraulic Engineering*, *110*(2), 197–199. https://doi.org/10.1061/(asce)0733-9429(1984)110:2(197)
Pillsbury, G. B. (1940). *Tidal hydraulics* (pp. 281). U.S. Army Corps Engineers, Vicksburg, Va.
Pritchard, D., & Hogg, A. J. (2003). Cross-shore sediment transport and the equilibrium morphology of mudflats under tidal currents. *Journal of Geophysical Research: Oceans*, *108*(10), 3313. https://doi.org/10.1029/2002jc001570
Pritchard, D., Hogg, A. J., & Roberts, W. (2002). Morphological modelling of intertidal mudflats: The role of cross-shore tidal currents. *Continental Shelf Research*, *22*(11–13), 1887–1895. https://doi.org/10.1016/S0278-4343(02)00044-4
Redolfi, M., Musa, M., & Guala, M. (2021). On steady alternate bars forced by a localized asymmetric drag distribution in erodible channels. *Journal of Fluid Mechanics*, *916*(A13), 1–35. https://doi.org/10.1017/jfm.2021.122
Redolfi, M., Welber, M., Carlin, M., Tubino, M., & Bertoldi, W. (2020). Morphometric properties of alternate bars and water discharge: A laboratory investigation. *Earth Surface Dynamics Discussions*, *8*(3), 1–31. https://doi.org/10.5194/esurf-2020-27
Redolfi, M., Zolezzi, G., & Tubino, M. (2016). Free instability of channel bifurcations and morphodynamic influence. *Journal of Fluid Mechanics*, *799*, 476–504. https://doi.org/10.1017/jfm.2016.389
Repetto, R., Tubino, M., & Paola, C. (2002). Planimetric instability of channels with variable width. *Journal of Fluid Mechanics*, *457*, 79–109. https://doi.org/10.1017/S0022112001007595
Rodrigues, S., Mosselman, E., Claude, N., Wintenberger, C. L., & Juge, P. (2015). Alternate bars in a sandy gravel bed river: Generation, migration and interactions with superimposed dunes. *Earth Surface Processes and Landforms*, *40*(5), 610–628. https://doi.org/10.1002/esp.3657
Schramkowski, G. P., Schuttelaars, H. M., & De Swart, H. E. (2002). The effect of geometry and bottom friction on local bed forms in a tidal embayment. *Continental Shelf Research*, *22*(11–13), 1821–1833. https://doi.org/10.1016/S0278-4343(02)00040-7
Schuttelaars, H. M., & de Swart, H. E. (1999). Initial formation of channels and shoals in a short tidal embayment. *Journal of Fluid Mechanics*, *386*, 15–42. https://doi.org/10.1017/s0022112099004395
Seminara, G. (1998). Stability and morphodynamics. *Meccanica*, *33*(1), 59–99. https://doi.org/10.1023/a:1004225516566
Seminara, G. (2010). Fluvial sedimentary patterns. *Annual Review of Fluid Mechanics*, *42*(1), 43–66. https://doi.org/10.1146/annurev-fluid-121108-145612
Seminara, G., Bolla Pittaluga, M., & Tambroni, N. (2012). Morphodynamic equilibrium of tidal channels. In W. Rodi, & M. Uhlmann (Eds.), *Environmental fluid mechanics: Memorial volume in honour of Prof. Gerhard H. Jirka* (pp. 153–174). CRC Press. https://doi.org/10.1201/b12283
Seminara, G., Lanzoni, S., Bolla Pittaluga, M., & Solari, L. (2001). Estuarine patterns: An introduction to their morphology and mechanics. *Geomorphological fluid mechanics* (pp. 455–499). Berlin: Springer Verlag. https://doi.org/10.1007/3-540-45670-8_19
Seminara, G., Lanzoni, S., Tambroni, N., & Toffolon, M. (2010). How long are tidal channels? *Journal of Fluid Mechanics*, *643*, 479–494. https://doi.org/10.1017/S0022112009992308
Seminara, G., & Tubino, M. (1989). Alternate bars and meandering: Free, forced and mixed interactions. In S. Ikeda, & G. Parker (Eds.), *River meandering* (pp. 267–320). American Geophysical Union. https://doi.org/10.1029/WM012p0267
Seminara, G., & Tubino, M. (2001). Sand bars in tidal channels. Part 1. Free bars. *Journal of Fluid Mechanics*, *440*, 49–74. https://doi.org/10.1017/S0022112001004748
Shaw, J. B., Miller, K., & McElroy, B. (2018). Island formation resulting from radially symmetric flow expansion. *Journal of Geophysical Research: Earth Surface*, *123*(2), 363–383. https://doi.org/10.1002/2017JF004464
Sittoni, L., Paola, C., & Voller, V. (2014). Geometry, flow, and sediment transport of alluvial deposits induced by topographically driven flow expansions. *Journal of Sedimentary Research*, *84*(2), 122–135. https://doi.org/10.2110/jsr.2014.11
Siviglia, A., Stecca, G., Vanzo, D., Zolezzi, G., Toro, E. F., & Tubino, M. (2013). Numerical modelling of two-dimensional morphodynamics with applications to river bars and bifurcations. *Advances in Water Resources*, *52*, 243–260. https://doi.org/10.1016/j.advwatres.2012.11.010
Slingerland, R. L., & Smith, N. D. (2004). River avulsions and their deposits. *Annual Review of Earth and Planetary Sciences*, *32*(1), 257–285. https://doi.org/10.1146/annurev.earth.32.101802.120201
Solari, L., Seminara, G., Lanzoni, S., Marani, M., & Rinaldo, A. (2002). Sand bars in tidal channels Part 2. Tidal meanders. *Journal of Fluid Mechanics*, *451*, 203–238. https://doi.org/10.1017/s0022112001006565
Struiksma, N., & Crosato, A. (1989). Analysis of a 2-D bed topography model for rivers. In S. Ikeda, & G. Parker (Eds.), *River meandering* (pp. 153–180). https://doi.org/10.1029/wm012p0153
Talmon, A. M., Struiksma, N., & Van Mierlo, M. C. L. M. (1995). Laboratory measurements of the direction of sediment transport on transverse alluvial-bed slopes. *Journal of Hydraulic Research*, *33*(4), 495–517. https://doi.org/10.1080/00221689509498657
Tambroni, N., Bolla Pittaluga, M., & Seminara, G. (2005). Laboratory observations of the morphodynamic evolution of tidal channels and tidal inlets. *Journal of Geophysical Research*, *110*(4), a–n. https://doi.org/10.1029/2004JF000243
Tambroni, N., Luchi, R., & Seminara, G. (2017). Can tide dominance be inferred from the point bar pattern of tidal meandering channels? *Journal of Geophysical Research: Earth Surface*, *122*(2), 492–512. https://doi.org/10.1002/2016JF004139
Tambroni, N., Seminara, G., & Paola, C. (2019). On the incipient formation of bars and channels on alluvial fans. *Earth Surface Processes and Landforms*, *44*(12), 2479–2493. https://doi.org/10.1002/esp.4676
Ter Brake, M. C., & Schuttelaars, H. M. (2011). Channel and shoal development in a short tidal embayment: An idealized model study. *Journal of Fluid Mechanics*, *677*, 503–529. https://doi.org/10.1017/jfm.2011.97
Todeschini, I., Toffolon, M., & Tubino, M. (2008). Long-term morphological evolution of funnel-shape tide-dominated estuaries. *Journal of Geophysical Research: Oceans*, *113*(5), 1–14. https://doi.org/10.1029/2007JC004094
Toffolon, M., & Lanzoni, S. (2010). Morphological equilibrium of short channels dissecting the tidal flats of coastal lagoons. *Journal of Geophysical Research*, *115*(4), 1–15. https://doi.org/10.1029/2010JF001673
Tubino, M. (1991). Growth of alternate bars in unsteady flow. *Water Resources Research*, *27*(1), 37–52. https://doi.org/10.1029/90WR01699
Tubino, M., Repetto, R., & Zolezzi, G. (1999). Free bars in rivers. *Journal of Hydraulic Research*, *37*(6), 759–775. https://doi.org/10.1080/00221689909498510

Tubino, M., & Seminara, G. (1990). Free-forced interactions in developing meanders and suppression of free bars. *Journal of Fluid Mechanics*, *214*(4), 131–159. https://doi.org/10.1017/s0022112090000088

van de Lageweg, W. I., & Feldman, H. (2018). Process-based modelling of morphodynamics and bar architecture in confined basins with fluvial and tidal currents. *Marine Geology*, *398*(January), 35–47. https://doi.org/10.1016/j.margeo.2018.01.002

van der Wegen, M., & Roelvink, D. J. (2008). Long-term morphodynamic evolution of a tidal embayment using a two-dimensional, process-based model. *Journal of Geophysical Research: Oceans*, *113*(3), 1–23. https://doi.org/10.1029/2006JC003983

van Leeuwen, S. M., & de Swart, H. E. (2001). The effect of advective processes on the morphodynamic stability of short tidal embayments. *Physics and Chemistry of the Earth, Part B: Hydrology, Oceans and Atmosphere*, *26*(9), 735–740. https://doi.org/10.1016/s1464-1909(01)00078-8

Van Oyen, T., & Blondeaux, P. (2009). Grain sorting effects on the formation of tidal sand waves. *Journal of Fluid Mechanics*, *629*, 311–342. https://doi.org/10.1017/S0022112009006387

Viparelli, E., Borhani, S., Torres, R., & Kendall, C. G. C. (2019). Equilibrium of tidal channels carrying nonuniform sand and interacting with the ocean. *Geomorphology*, *329*, 1–16. https://doi.org/10.1016/j.geomorph.2018.12.017

Welford, M. R. (1994). A field test of Tubino's (1991) model of alternate bar formation. *Earth Surface Processes and Landforms*, *19*(4), 287–297. https://doi.org/10.1002/esp.3290190402

Wu, F. C., Shao, Y. C., & Chen, Y. C. (2011). Quantifying the forcing effect of channel width variations on free bars: Morphodynamic modeling based on characteristic dissipative Galerkin scheme. *Journal of Geophysical Research*, *116*(3), 1–20. https://doi.org/10.1029/2010jf001941

Yu, Q., Wang, Y., Gao, S., & Flemming, B. (2012). Modeling the formation of a sand bar within a large funnel-shaped, tide-dominated estuary: Qiantangjiang Estuary, China. *Marine Geology*, *299–302*, 63–76. https://doi.org/10.1016/j.margeo.2011.12.008

Zolezzi, G., Guala, M., Termini, D., & Seminara, G. (2005). Experimental observations of upstream overdeepening. *Journal of Fluid Mechanics*, *531*, 191–219. https://doi.org/10.1017/s0022112005003927